

Does the Sun Appear Brighter at Night in Neutrinos?

J.N. Bahcall and P.I. Krastev

School of Natural Sciences, Institute for Advanced Study

Princeton, NJ 08540

We calculate accurately the number of solar neutrino events expected as a function of solar zenith angle, with and without neutrino oscillations, for detectors at the locations of Super-Kamiokande, SNO, and the Gran Sasso National Laboratory. Using different earth models to estimate geophysical uncertainties, and different solar models to estimate solar uncertainties, we evaluate distortions predicted by the MSW effect in the zenith angle distributions of solar neutrino events. The distortions are caused by oscillations and by $\nu - e$ interactions in the earth that regenerate ν_e from ν_μ or ν_τ . We show that the first two moments of the zenith-angle distribution are more sensitive to the small mixing angle MSW solution than the conventionally studied day-night asymmetry. We present iso-sigma contours that illustrate the potential of Super-Kamiokande, SNO, BOREXINO, ICARUS and HERON/HELLAZ for detecting the earth regeneration effect at their actual locations (and at the equator). MSW solutions favored by the four pioneering solar neutrino experiments predict characteristic distortions for Super-Kamiokande, SNO, BOREXINO, and ICARUS that range from being unmeasurably small to $> 5\sigma$ (stat) after only a few years of observations.

arXiv:hep-ph/9706239v2 16 Sep 1997

I. INTRODUCTION

Four operating solar neutrino experiments (Chlorine [1], Kamiokande [2], GALLEX [3]) and SAGE [4] have detected neutrinos from nuclear fusion in the interior of the sun with approximately the numbers and energies expected from standard solar models [5,6]. Moreover, sound speeds calculated from the standard solar models agree with the helioseismologically determined sound speeds to a rms accuracy of better than 0.2% throughout essentially the entire sun [7].

Nevertheless, quantitative discrepancies have persisted for almost three decades between the predictions of the standard solar models and the observations of solar neutrino experiments [8–10]. Several suggested modifications of neutrino properties provide excellent fits to the existing solar neutrino data [11].

Are there potential “smoking gun” indications of new physics? Yes, the most popular neutrino physics solution, the Mikheyev-Smirnov-Wolfenstein (MSW) effect [12], predicts several characteristic and unique phenomena. The MSW effect explains solar neutrino observations as the result of conversions in the solar interior of ν_e produced in nuclear reactions to the more difficult to detect ν_μ or ν_τ .

Potentially decisive signatures of new physics that are suggested by the MSW effect include observing that the sun is brighter in neutrinos at night (the ‘earth regeneration effect’) [13–15], detecting distortions in the incident solar neutrino energy spectrum [16], and observing that the flux of all types of neutrinos exceeds the flux of just electron type neutrinos [17,18]. A demonstration that any of these phenomena exists would provide evidence for physics beyond the minimal standard electroweak model.

The regeneration effect is an especially powerful diagnostic of new physics since no difference is predicted between the counting rates observed during the day and at night (or, more generally, any dependence of the counting rate on the solar zenith angle) by such popular alternatives to the MSW effect as vacuum oscillations [19], magnetic moment transitions [20], or violations of the equivalence principle [21].

In this paper, we investigate the sensitivity of new solar neutrino experiments, Super-Kamiokande [22], SNO [23], ICARUS [24], BOREXINO [25], HERON [26] and HELLAZ [27], to the earth regeneration effect. The MSW effect predicts that, for certain values of the neutrino masses and mixing angles, $\nu - e$ interactions in the earth (at night) may convert ν_μ or ν_τ from the sun back into the more easily detectable ν_e .

An accurate evaluation of the systematic significance of experimental results will require the detailed Monte Carlo simulations that will be carried out by the experimental collaborations; the collaborations will determine the best estimates and uncertainties for all the quantities that affect the experimental result. These results will then be analyzed using computer codes that include the experimental details and which make use of optimal statistical techniques such as maximum likelihood analysis. In the absence of detailed Monte Carlo simulations of the experimental characteristics (yet to be determined), we estimate in this paper the statistical significance of expected results by comparing the predictions of various MSW scenarios with respect to the no-oscillation scenario including only statistical errors and analyzing the results with a χ^2 statistic.

The reader who wants to see the approximate power of the new experiments can turn immediately to Fig. 9, which shows the significance level (statistical errors only) with which new solar experiments could detect the regeneration effect. Experience with the operating experiments over a period of years may be necessary to determine the size of the systematic errors.

This paper is organized as follows. In Sec. II we summarize the general features of ν_e regeneration in the earth. We then describe in Sec. III the different models of the earth used for estimating the uncertainties in the numerical calculations due to uncertainties in the density profile and the chemical composition of the earth's interior. In the detailed calculations that follow, we use the differences between the results obtained from the different models of the earth to determine the geophysical uncertainties in the MSW predictions.

After these preliminary considerations, we determine in Sec. IV the regions in the mixing angle and mass difference plane, $\sin^2 2\theta - \Delta m^2$, that are allowed by the latest solar neutrino

data, taking into account the influence of earth regeneration on the predicted counting rates in the chlorine, Kamiokande, GALLEX, and SAGE experiments. In addition to the familiar large mixing angle and small mixing angle MSW solutions, we find an additional LOW solution (large mixing angle, smaller neutrino mass difference) that has an acceptable confidence level only when earth regeneration is included in the calculations.

We then investigate the sensitivity of next-generation solar neutrino experiments to the earth regeneration effect. We begin by defining and calculating the zenith-angle exposure function in Sec. V. This function depends only on the location of a neutrino detector on the surface of the earth; it is independent of the characteristics of the detector. We also calculate in Sec. V the distorted zenith angle distribution that takes account of regeneration in the earth.

The results for MSW regeneration given previously in the literature involve making approximations either in the model description of the earth or in the calculation of the average survival probability after regeneration, or both. Instead, we integrate numerically the differential equations describing the evolution of the neutrino states in traversing an accurate model of the earth, thereby avoiding the necessity of arguing that an approximation scheme is sufficiently accurate. In several tables in this paper, we present numerical results to a precision of 0.01%, an accuracy much higher than can be measured experimentally. These precise numerical predictions are given in order to illustrate the small effect on measurable quantities of some of the systematic differences.

We introduce in Sec. VI the first two moments of the zenith-angle distribution of neutrino events and calculate the dependence of the moments on neutrino parameters for the new solar neutrino experiments: Super-Kamiokande, SNO, ICARUS, BOREXINO and HERON/HELLAZ. For comparison, we calculate accurately in Sec. VII the conventional day-night asymmetry; we present values of the day-night asymmetry for the new solar neutrino detectors mentioned above.

Which characterization is more sensitive to new physics: the moments of the zenith-angle distribution or the day-night asymmetry? We show in Sec. VIII that the moments are more

sensitive to the small mixing angle MSW solution and the day-night asymmetry is more sensitive to the large mixing angle solution. Although less statistically powerful than the full Monte Carlo simulations that will be carried out by the experimental collaborations, the analyses using, e. .g, moments or the day-night asymmetry can be carried out quickly by theoreticians interested in determining whether new particle physics scenarios can be tested by the experiments or whether they are already inconsistent with data that have been published. For completeness, we present in Sec. IX the moments of the electron recoil energy spectrum for Super-Kamiokande and SNO that were computed including the earth regeneration effect.

We then show in Sec. X that the MSW predictions for regeneration in the earth depend only slightly on the adopted density profile of the earth, the chemical composition of the earth, and the details of the solar model.

Following the suggestion of Gelb, Kwong, and Rosen [28], we calculate in Sec. XI the increase in the sensitivity to the regeneration effect that could be achieved by building detectors at the equator. We discuss and summarize our main results in Sec. XII.

II. THE EARTH REGENERATION EFFECT

We work in a two-neutrino mixing scheme involving ν_e (produced in the sun) and either ν_μ or ν_τ (produced by oscillations). Soon after Mikheyev and Smirnov suggested the MSW effect [12] as a possible solution of the solar neutrino problems, several authors pointed out [13] that day-night variations of the event rates in solar neutrino detectors could provide spectacular confirmation of the MSW effect and thus of new physics.

The MSW solution of the solar neutrino problems requires that electron neutrinos produced in nuclear reactions in the center of the sun are converted to muon or tau neutrinos by interactions with solar electrons on their way from the interior of the sun to the detector on earth. The conversion in the sun is primarily a resonance phenomenon, which occurs at a specific density that corresponds to a definite neutrino energy (for a specified neutrino mass

difference).

During day-time, the higher-energy neutrinos arriving at earth are mostly ν_μ (or ν_τ) with some admixture of ν_e . At night-time, neutrinos must pass through the earth in order to reach the detector. As a result of traversing the earth, the fraction of the more easily detected ν_e increases because of the conversion of ν_μ (or ν_τ) to ν_e by neutrino oscillations. For the small mixing angle MSW solution, interactions with electrons in the earth increase the effective mixing angle and enhance the conversion process. For the large mixing angle MSW solution, the conversion of ν_μ (or ν_τ) to ν_e occurs by oscillations that are only slightly enhanced over vacuum mixing. This process of increasing in the earth the fraction of the neutrinos that are ν_e is called the “regeneration effect” and has the opposite effect to the conversion of ν_e to ν_μ (or ν_τ) in the sun.

Because of the change of neutrino type in the earth, the MSW mechanism predicts that solar neutrino detectors should generally measure higher event rates at night than during day-time.

Figure 1 illustrates a schematic view of a solar neutrino detector at the geographic latitude, ϕ . Since the earth is spherically symmetric to $O(10^{-2.5})$, it is sufficient to consider the cross-section slice shown in the figure.* Two lines determine the geometry: one line defines the zenith direction, and the other line is the trajectory of the neutrino. The zenith angle α ($0^\circ < \alpha < 180^\circ$) between these two lines specifies the neutrino trajectory in the earth. The survival probability depends on the neutrino oscillation parameters, Δm^2 and $\sin^2 2\theta$, on the neutrino energy, E , and on the path (i.e., α) the neutrino travels through the earth. Since α changes due to the apparent motion of the sun, the neutrino survival probability should change with time as well, resulting in an asymmetric distortion of the angular distribution of events.

*The polar-equatorial asymmetry of the earth changes the predicted MSW regeneration effects by less than or of order 0.3%, which is not observable with existing or planned detectors.

Real-time detectors, which record the times at which neutrinos interact within the detector, are best suited for studying the earth regeneration effect. In radiochemical experiments the time of detection is poorly known, since a typical run usually lasts between several weeks (gallium) and several months (chlorine).[†]

Kamiokande, a real-time neutrino electron scattering detector, did not see any signal for the earth regeneration effect. The Kamiokande collaboration used this non-observation to rule out an important region in parameter space for which the predicted day-night asymmetry, or zenith-angle dependence, is large [30]. However, the sensitivity of the Kamiokande detector was insufficient to probe the full $\Delta m^2 - \sin^2 2\theta$ parameter space for which there might be an appreciable day-night effect, measurable by Super-Kamiokande or SNO.

There are several calculations in the literature [31–35] of the expected magnitude of the regeneration effect in future experiments. Different groups of researchers have used different models of the earth in their calculations. No quantitative estimate has been made previously of the sensitivity of the measurable quantities to the adopted density profile of the earth; each group has typically presented results using a specific density profile, often not the best available profile. In the subsequent sections, we describe direct numerical computations of the earth regeneration effect for six different models of the earth. Thus we quantify the dependence of the calculated characteristics of the earth regeneration effect on the model of the earth and exhibit the corresponding uncertainties which turn out to be rather small. The density profiles in the six models of the earth are described in Sec. III.

III. EARTH MODELS

The MSW effect in the earth depends upon the electron number density as a function of radius. In this section, we determine best-estimates and a range of uncertainties for the

[†]The possibility of making extractions twice a day and counting separately day-time and night-time samples in the chlorine and iodine experiments has been considered carefully. [29].

total mass density and for the chemical composition. We use the best available earth models and chemical composition for most of the calculations performed in this paper, but we also carry out calculations for five older mass models in order to determine the uncertainties in the predicted MSW effects that arise from uncertainties in the model of the earth’s density profile. We use a best-estimate chemical composition for the core that is inferred from the seismological measurements. To test the sensitivity of the MSW predictions to the assumed chemical composition of the earth, we make extreme assumptions that maximize or minimize the average charge to mass ratio and carry out calculations also for these extreme cases.

A. Density Profiles

The density distribution inside the earth is known with a precision of a few percent [36]. A large set of seismic measurements has been used to obtain the most accurate model, PREM [37] (the Preliminary Reference Earth Model), for the earth’s density distribution. We will use the PREM model for all of our best-estimate calculations. This model has also been used by Lisi and Montanino [34] as the basis of their recent analytic study of earth regeneration. Other models are described in Refs. [38] and [39]. To determine the sensitivity to the assumed density profile, we have performed calculations with a representative set of six different earth models, all spherically symmetric and with the same radius, $R_{\oplus} = 6371$ km.

Figure 2 shows the density profiles of the six earth models. The density distributions in these models are divided into five zones: a) a crust with a thickness of a few tens of kilometers, b) an upper mantle extending down from the crust to about 1000 km, c) a lower mantle down to about 2900 km, d) an outer core between 1250 km and 3480 km from the center, and e) an inner core of radius ≈ 1220 km. The density changes abruptly between the inner and outer core, and also at the border between the lower mantle and the outer core. The positions of these abrupt changes are known with an accuracy of better than a percent from seismological data.

Table I compares the mass and moment of inertia that we have computed for each of the six earth models with the measured values. The recent models given in [37] and [39] reproduce the total mass and moment of inertia with excellent precision. The older models [40–43] give slightly worse fits to the mass and moment of inertia. The models listed in the third to sixth row in Table I are in conflict with seismological measurements.

The set of six models represents a sample that allows for variations of the density distribution larger than the uncertainties in the PREM model. As shown in Sec. VI (and the last four columns of Table I), the large differences between the six density models produce relatively small (but not always negligible, see Sec. VI) changes in the predicted characteristics of the earth regeneration effect for the Super-Kamiokande, SNO, BOREXINO, ICARUS, and HERON/HELLAZ experiments.

Figure 2 shows that the largest differences between the six models of the earth are in the core, below 2000 km. The operating solar neutrino experiments, and those currently under development, are located at relatively high northern latitudes. Solar neutrinos that are detected in these experiments never cross the inner core of the earth. Among the real-time experiments that are currently operating or are under construction, Super-Kamiokande is most sensitive to the core distribution. Nevertheless, the fraction of a year during which the neutrinos cross the outer core at the Kamioka site is small ($\simeq 7\%$).

B. Chemical Compositions

Measurements of the propagation of seismological waves in the earth’s interior and studies of the properties of minerals under high pressure, have been combined to determine the chemical composition of the earth’s interior with relatively high accuracy [44,45]. Using the results of references [44,45], we adopt a best-estimate charge to mass ratio, Z/A , of 0.468 for the core (83% Fe, 9% Ni, and 8% light elements with $Z/A = 0.5$) and 0.497 for the mantle (41.2% SiO₂, 52.7% MgO and 6.1% FeO).

A lower limit for the charge to mass ratio in the core is 0.465, which corresponds to

assuming a composition of 100% iron. From the seismic and mineral data, geophysicists have concluded [44] that the minimum amount of iron in the core is 80%. We determine a maximum value of $Z/A = 0.472$ in the core by assuming a composition of 80% iron and 20% light elements. The total range of the electron number density due to the imperfectly known composition of the core is about 1.5%.

The chemical composition in the mantle is believed known to about 1% (see ref. [36]). We consider here variations of -1% and -2% . The value of Z/X in the mantle cannot be increased significantly above the standard value of 0.496 because that would require the presence of a large amount of hydrogen in the mantle.

IV. AVERAGE EVENT RATES AND MSW SOLUTIONS

Including the earth regeneration effect, we have calculated the expected one-year average event rates as functions of the neutrino oscillation parameters Δm^2 and $\sin^2 2\theta$ for all four operating experiments which have published results from their measurements of solar neutrino event rates. These include the chlorine experiment, Kamiokande, GALLEX and SAGE. Thus we update our previous results given in Ref. [11], in which the earth effect was neglected. We take into account, as before, the known threshold and cross-section for each detector. In the case of Kamiokande, we also take into account the known energy resolution ($20\% \ 1\sigma$ at electron energy 10 MeV) and trigger efficiency function [46].

We first calculate the one year average survival probability, \bar{P}_{SE} , for a large number of values of Δm^2 and $\sin^2 2\theta$ using the method described in Appendix A. Then we compute the corresponding one year average event rates in each detector. We perform a χ^2 analysis taking into account theoretical uncertainties and experimental errors as described in [47].

Table II summarizes the reported mean event rates from each detector. We obtain allowed regions in $\Delta m^2 - \sin^2 2\theta$ parameter space by finding the minimum χ^2 and plotting contours of constant $\chi^2 = \chi_{min}^2 + \Delta\chi^2$ where $\Delta\chi^2 = 5.99$ for 95% C.L. and 9.21 for 99%

C.L. ‡.

The best fit is obtained for the small mixing angle (SMA) solution:

$$\Delta m^2 = 5.0 \times 10^{-6} \text{eV}^2, \quad (1a)$$

$$\sin^2 2\theta = 8.7 \times 10^{-3}, \quad (1b)$$

which has a $\chi_{\min}^2 = 0.25$. There are two more local minima of χ^2 . The best fit for the well known large mixing angle (LMA) solution occurs at

$$\Delta m^2 = 1.3 \times 10^{-5} \text{eV}^2, \quad (2a)$$

$$\sin^2 2\theta = 0.63, \quad (2b)$$

with $\chi_{\min}^2 = 1.1$. There is also a less probable solution, which we refer to as the LOW solution (low probability, low mass), at [48,31]

$$\Delta m^2 = 1.1 \times 10^{-7} \text{eV}^2, \quad (3a)$$

$$\sin^2 2\theta = 0.83. \quad (3b)$$

with $\chi_{\min}^2 = 6.9$. The LOW solution is acceptable only at 96.5% C.L.

Figure 3 shows the allowed regions in the plane defined by Δm^2 and $\sin^2 2\theta$. The C.L. is 95% for the allowed regions of the SMA and LMA solutions and 99% for the LOW solution. The black dots within each allowed region indicate the position of the local best-fit point in parameter space. The results shown in Fig. 3 were calculated using the predictions of the 1995 standard solar model of Bahcall and Pinsonneault [6], which includes helium and heavy element diffusion; the shape of the allowed contours depends only slightly upon the assumed solar model (see Fig. 1 of ref. [11]).

The results given here differ somewhat from those given earlier in ref. [11], both because we are now including the regeneration effect and also because we are using more recent experimental data for the pioneering solar neutrino experiments. Comparing the results

‡The C.L. in this paper are always for two degrees of freedom. The values of χ^2 are not reduced.

given in Eqs. (1)–(3) and Figs. 3 with the corresponding allowed regions obtained for the same input neutrino experimental data but without including the earth effect shows that terrestrial regeneration changes only slightly the best-fit solutions for the SMA solution ($\lesssim 5\%$ in Δm^2 and $\sin^2 2\theta$) and the LMA solution ($\lesssim 10\%$ in Δm^2 and $\sin^2 2\theta$). The values of χ_{\min}^2 are also not significantly affected. The LOW solution is acceptable only if the regeneration effect is included; otherwise, the LOW solution is ruled out at 99.9% C.L.

Figure 4 compares the computed survival probabilities for the day (no regeneration), the night (with regeneration), and the annual average. These results are useful in understanding the day-night shifts in the energy spectrum that are computed and discussed in Sec. IX. The results in the figure refer to a detector at the location of Super-Kamiokande, but the differences are very small between the survival probabilities at the positions of Super-Kamiokande, SNO, and the Gran Sasso Underground Laboratory.

V. THE ZENITH-ANGLE EXPOSURE FUNCTION AND THE ZENITH-ANGLE DISTRIBUTION FUNCTION

In this section, we define and calculate the zenith-angle exposure function and show how the exposure function can be distorted by oscillations and by neutrino-electron interactions in the earth into the zenith-angle distribution function.

The fractional number of neutrino events observed as a function of solar zenith angle, α (see Fig. 1), is, for standard neutrino physics, determined only by the latitude of the neutrino detector. The number of events is largest for zenith angles at which the sun spends the most time in its apparent motion around the earth. In what follows, we shall refer to the normalized number distribution of events, $Y(\alpha)$, as the “zenith-angle exposure function”; this function describes the relative amount of time the detector is exposed to the sun at a fixed zenith angle. We present in this section the zenith-angle exposure function calculated assuming massless neutrinos (no oscillations) and detectors placed at Kamioka, Japan (Kamiokande and Super-Kamiokande), Sudbury, Canada (SNO), and the Gran Sasso

Underground Laboratory (GALLEX, ICARUS, BOREXINO and HERON/HELLAZ). The exposure function for the Homestake detector has been calculated by Cherry and Lande [13].

The zenith-angle distribution of events can be distorted by the earth regeneration effect implied by MSW solutions, since at solar zenith angles larger than 90° neutrinos pass through the earth on their way to the detector and therefore ν_e 's can be regenerated by interactions with electrons in the earth's interior. The distorted distribution function, $f(\alpha)$, will be referred to as the "zenith-angle distribution." The main goal of this paper is to calculate and analyze the shape of $f(\alpha)$ predicted by different MSW solutions and to estimate the sensitivity of detectors to the difference between $f(\alpha)$ and the zenith-angle exposure function, $Y(\alpha)$.

A. Zenith-Angle Exposure Function

In order to represent accurately the zenith-angle exposure function, we consider 360 angles, α_i , separated by 0.5° intervals between 0 and 180° . The fraction of time in a year during which the zenith angle, α , (see Fig. 1) of the sun is close to α_k is proportional to:

$$Y'(\alpha_k) = \sum_{i=1}^N \theta(\alpha(t_i) - \alpha_k) \theta(\alpha_{k+1} - \alpha(t_i)) [1 \text{ AU}/R(t_i)]^{-2}. \quad (4)$$

Here $\alpha(t_i)$ is the solar zenith angle at time t_i , $N = T/\Delta t$, T is the duration of one calendar year, and Δt is the time-step. The function θ is the well known step-function $\theta(x) = 0$, $x < 0$ and $\theta(x) = 1$, $x \geq 0$. The function $R(t)$ is the instantaneous earth-sun distance, and 1 AU is the one year average earth-sun distance for which solar neutrino fluxes are routinely calculated in standard solar models (see Appendix B for an explicit representation of the time-dependent earth-sun distance).

The sum in Eq. (4) was computed by simulating the motion of the sun on the celestial sphere during one calendar year using the formulae in Appendix B. Computations with different time steps between a few seconds to a few minutes are practically equivalent for calculating event rates in the various solar neutrino detectors.

The normalized zenith-angle exposure function, $Y(\alpha_k)$, is obtained directly from Eq. (2),

$$Y(\alpha_k) = Y'(\alpha_k) / \sum_{i=1}^N Y'(\alpha_i). \quad (5)$$

Thus $Y(\alpha_k)$ is the fraction of the time during one calendar year that the sun's zenith angle is within the interval $(\alpha_k - 0.25^\circ, \alpha_k + 0.25^\circ)$. If the solar neutrino flux is constant in time (no neutrino oscillations occur), then the function $Y(\alpha)$ will be the normalized angular distribution of events in the detector. We use the analytical expressions for $R(t)$ given in Ref. [49] (see Eq. B2). The zenith angle exposure function was calculated analytically in ref. [34], without including the variation due to the changing earth-sun distance.

Figures 5 and 6 show the undistorted zenith-angle exposure functions for Super-Kamiokande, SNO, and, the detectors assumed to operate at Gran Sasso (ICARUS, BOREXINO, and HERON/HELLAZ). Convenient numerical tables for the $Y(\alpha_k)$ are available at <http://www.sns.ias.edu/~jnb>. Table III lists the latitudes (all northern) of each of the solar neutrino detectors.

The positions of the sharp peaks in Figs. 5 and 6 are determined by the location of the detector and by the obliquity, ϵ , of the earth's orbit (approximately 23.4°). The absolute value of the difference between the maximum (or minimum) possible zenith angle for a given location and the position of the closest peak is equal to $\phi + \epsilon$. At summer solstice, the sun's zenith angle changes from the minimum possible to the angle corresponding to the second peak (at an angle $> 90^\circ$). At winter solstice the sun goes between the peak at angle $< 90^\circ$ and the maximum possible zenith angle. Thus during winter solar neutrinos pass closer to the earth's center, whereas during summer they go through lower density layers of the mantle.

B. Zenith-Angle Distribution Function

We calculate the event rates, Q_i , along each direction, α_i , with the aid of a set of survival probabilities, P_{SE}^i , computed (just once for each direction, mixing angle, and $E/\Delta m^2$) along

a fixed set of trajectories through the earth. The numerical value of each Q_i is obtained from Eq. C1 of Appendix C. The normalized zenith-angle distribution function is

$$f(\alpha_i) = Q(\alpha_i)Y(\alpha_i) / \sum_k Q(\alpha_k)Y(\alpha_k). \quad (6)$$

In the absence of oscillations, the detector event rate, Q_i , is independent of direction and disappears from the right-hand side of the equation. In this case $f(\alpha) \equiv Y(\alpha)$.

In Figs. 5 and 6, we present the expected distorted angular distributions for the SMA, LMA, and LOW solutions in Super-Kamiokande, SNO, ICARUS, BOREXINO and HERON/HELLAZ. In the panels for Super-Kamiokande, SNO and ICARUS, we show only the distributions corresponding to the best-fit points in the SMA and LMA solutions; the curves corresponding to the LOW solution are virtually undistorted. Correspondingly, in the panels for BOREXINO and HERON/HELLAZ, we show only the expected angular distribution for the LOW solution (see Eq. 3b), since the SMA and LMA solutions imply only a negligible distortion of the zenith-angle distribution for these low energy detectors.

VI. MOMENTS OF THE ZENITH-ANGLE DISTRIBUTION

In this section, we evaluate the expected MSW distortions of the angular distribution and compare the first two moments of the predicted angular distribution of events with the calculated moments expected in the absence of oscillations. This comparison constitutes a new and, for the small mixing angle solution, a more powerful way of analyzing the time dependence of the observed neutrino events. The predicted distortions of the recoil electron energy spectra in Super-Kamiokande and in SNO were investigated in Ref. [50,34] in terms of the analogous moments of the energy distribution.

In Sec. VIA, we define the first and second moments of the zenith-angle distribution and then calculate in Sec. VIB the predicted MSW changes in the zenith-angle distributions. We plot the relative shift of the first moment in the plane of the neutrino oscillation parameters Δm^2 and $\sin^2 2\theta$, illustrating the range of possible values of the shift of the first moment

within the 95% C.L. allowed by the Chlorine [1], Kamiokande [2], GALLEX [3], and SAGE [4] experiments.

How sensitive will the Super-Kamiokande, SNO, ICARUS, BOREXINO and HELLAZ/HERON experiments be to the regeneration effect? We answer this question in Sec. VIB by plotting the number of standard deviations each MSW solution is separated from the no-oscillation solution in the plane defined by the values of the first two moments.

A. Moment Definitions

The first two moments of the zenith-angle distribution are defined by

$$\langle \alpha \rangle = \int \alpha f(\alpha) d\alpha, \quad (7a)$$

and

$$\sigma^2 = \int (\alpha - \langle \alpha \rangle)^2 f(\alpha) d\alpha. \quad (7b)$$

The fractional shifts in these two moments are defined as

$$\frac{\Delta \langle \alpha \rangle}{\alpha_0} = (\langle \alpha \rangle - \alpha_0) / \alpha_0, \quad (8a)$$

and

$$\frac{\Delta \sigma^2}{\sigma_0^2} = (\sigma^2 - \sigma_0^2) / \sigma_0^2, \quad (8b)$$

where α_0 and σ_0^2 are the moments of the zenith-angle exposure function distribution (no oscillations) and $\langle \alpha \rangle$ and σ^2 are the moments of the distorted (by oscillations) zenith-angle distribution. Because of the symmetry of $Y(\alpha)$ about $\alpha = 90$ deg, $\alpha_0 = \pi/2$ for all the detector locations. The values of the undistorted second moment, σ_0 , are: 37.9° (Super-Kamiokande), 32.9° (SNO), 34.9° (Gran Sasso), 33.9° (Homestake), 34.5° (Baksan), and 47.5° (Equator).

The Kamiokande collaboration excluded a significant region in $\Delta m^2 - \sin^2 2\theta$ parameter space by grouping the events from below the horizon into five bins, corresponding to different

zenith angles [2]. Lisi and Montanino in Ref. [34] calculated binned angular distributions for Super-Kamiokande and SNO for different values of Δm^2 and θ^2 .

The calculation of the first two moments of the zenith-angle distribution is subject to fewer complications than the more traditional method used in references [2,34] of binning the data and doing a χ^2 analysis. For binned data, the *a priori* unknown normalization and the angular dependence of the detector sensitivity are, for example, two of the aspects of neutrino experiments that introduce bin-to-bin correlations which are often difficult to estimate from the observations or to evaluate including all of the relevant detector characteristics. On the other hand, the calculation of the first and second moments directly from the data is straightforward.

B. Predicted MSW Moments

Figures 7 and 8 show the expected shifts in the first two moments as a function of the neutrino oscillation parameters, Δm^2 and $\sin^2 2\theta$. We plot in Fig. 7 (Fig. 8) contours of constant fractional shift, $\Delta\alpha/\alpha_0$ ($\Delta\sigma^2/\sigma_0^2$), of the first moment (second moment) in the Δm^2 - $\sin^2 2\theta$ plane. The five panels are, for both figures, for Super-Kamiokande, SNO, ICARUS, BOREXINO and HERON/HELLAZ. For Super-Kamiokande, $\Delta\alpha/\alpha_0$ varies between -0.1% and 3% in the SMA region and between 0.5% and 7% in the LMA region. The corresponding ranges for SNO are $(-0.1, 4.5)\%$ (SMA) and $(0.3, 15)\%$ (LMA). SNO is somewhat more sensitive than Super-Kamiokande to the shift of the first moment because $\nu_{\mu s}$ (and $\nu_{\tau s}$) do not contribute to the charged-current signal in SNO. ICARUS and SNO have similar sensitivities to the regeneration effect since both observe charged current reactions with high-energy thresholds of 10.9 MeV and 6 MeV, respectively. The low-energy experiments, BOREXINO and HERON/HELLAZ, are insensitive to both the SMA and LMA allowed regions, but will be able to test the LOW solution to which neither SNO nor Super-Kamiokande are sensitive. The results for the second moment, shown in Fig. 8, exhibit similar trends.

Figure 9 summarizes the potential of the second generation of solar neutrino experiments

for discovering new physics via the earth regeneration effect. The figure displays iso-sigma ellipses, statistical errors only, in the plane of the fractional percentage shifts of the first two moments, $\Delta\alpha/\alpha_0$ and $\Delta\sigma^2/\sigma_0^2$. Assuming a total number of events of 30000, (which corresponds to ~ 5 years of standard operation for Super-Kamiokande and ~ 10 years for SNO), we have computed the sampling errors on the first two moments as well as the correlation of the errors using the following well known formulae [51]: $\sigma(m_1) = \sqrt{\frac{\mu_2}{N}}$, $\sigma(m_2) = \sqrt{\frac{\mu_4 - \mu_2^2}{N}}$, and $\rho(m_1, m_2) = \frac{\mu_3}{\sqrt{\mu_2}\sqrt{\mu_4 - \mu_2^2}}$. Here μ_i is the i -th moment of the angular distribution of events and m_i are the corresponding estimates of the moments from a sample of size N (number of events). The iso-sigma ellipses for the six detectors we consider here are centered around the undistorted zenith-angle exposure function for which, by definition, $\Delta\alpha = \Delta\sigma^2 = 0$. Figure 9 shows for each detector the predicted shifts of the first two moments in the SMA, LMA, and LOW solutions. The horizontal and vertical error-bars denote the spread in predicted values of the shifts in the first two moments, which are obtained by varying Δm^2 and $\sin^2 2\theta$ within the 95% C.L. allowed (see Fig. 3) by the four pioneering solar neutrino experiments.

For Super-Kamiokande (SNO), the current best-fit parameters Δm^2 and $\sin^2 2\theta$ [see Eq. (9)] predict a 5σ (6.5σ) effect for the SMA solution and 13σ (25σ) effect for the LMA solution. Note that SNO is expected to require twice as much time to collect the same number of events as Super-Kamiokande. In the same amount of observing time, SNO and Super-Kamiokande are approximately equivalent for the SMA and Super-Kamiokande is significantly more efficient for the LMA.

VII. DAY-NIGHT ASYMMETRY

In this section, we calculate the day-night asymmetry [13–15,31,33–35] caused by the earth regeneration effect. For Super-Kamiokande and SNO, the first accurate calculations of the day-night asymmetry have been made only recently using a realistic density distribution in the earth [33,34].

We evaluate numerically the day-night asymmetry for Super-Kamiokande, SNO, ICARUS, BOREXINO, and HERON/HELLAZ. We present quantitative estimates of the sensitivity of future experiments to the predicted difference in night-time and day-time event rates.

The day-night asymmetry is defined as:

$$A_{n-d} = \frac{Q_n - Q_d}{Q_n + Q_d}, \quad (9)$$

where Q_n and Q_d are respectively the average night-time and day-time event rates during one year. The calculation of the asymmetry is made using the one-year average night-time and day-time survival probabilities described in Appendix A.

Figure 10 shows contours of constant day-night asymmetry in the $\Delta m^2 - \sin^2 2\theta$ plane for Super-Kamiokande, SNO, ICARUS, BOREXINO, and HERON/HELLAZ. The shaded regions in the panels for Super-Kamiokande, SNO, and ICARUS are allowed (at 95% C.L.) by the present data from Homestake, Kamiokande, GALLEX and SAGE. In order to include the LOW solution near $\Delta m^2 = 10^{-7}$ eV², the panels corresponding to BOREXINO and HERON/HELLAZ show the allowed regions at 99% C.L.

Table V gives the expected range of day-night asymmetries in Super-Kamiokande and SNO for both the SMA and LMA solutions. The ICARUS sensitivity is similar to SNO. In general, SNO is slightly more sensitive than Super-Kamiokande for testing the day-night asymmetry because SNO detects a CC reaction; the sensitivity to NC scattering of muon neutrinos decreases somewhat the sensitivity of the Super-Kamiokande detector. Both detectors are very sensitive to the large day-night asymmetry predicted in the LMA solution. Their sensitivity to the SMA solution is smaller, especially in the low $\sin^2 2\theta$ corner ($\sin^2 2\theta < 5 \times 10^{-3}$), where $A_{n-d} \simeq 0$. Both Super-Kamiokande and SNO are practically insensitive to the LOW solution because they can register only high-energy boron neutrinos which do not resonate in the earth for the low Δm^2 values in the LOW solution. As noted in Ref. [31], A_{n-d} is negative in a small region of parameter space for both Super-Kamiokande and SNO, i.e., the night time event rate can be slightly lower than the day-time event rate.

The differences between SNO and ICARUS are mainly due to the different assumed neutrino thresholds (6.4 MeV and 10.9 MeV, respectively) and to the locations of the detectors. For large mixing angles, for which the regeneration effect takes place mainly in the mantle, the sensitivities of the two detectors are particularly similar. At small mixing angles ($\sin^2 2\theta < 0.3$) and $5 \times 10^{-6} < \Delta m^2/\text{eV}^2 < 10^{-5}$, ICARUS is slightly more sensitive to the earth effect because it is located at a lower latitude than SNO.

The three future detectors that will measure low-energy neutrinos, BOREXINO (${}^7\text{Be}$), HERON (pp), and HELLAZ (pp), will be sensitive to the large day-night asymmetries predicted in the LOW solution, but insensitive to the asymmetries predicted by the SMA and LMA solutions. The range of day-night asymmetries expected for the LOW solution are ($16 \pm 5\%$) for HERON/HELLAZ and ($16 \pm 8\%$) for BOREXINO.

VIII. WHICH STATISTICAL TEST IS BEST?

Which statistical tests are most powerful in detecting new physics? What type of analysis will most clearly show departures from the zenith-angle exposure function due to the regeneration effect? By analyzing simulated data in this section, we shall see that the preferred statistical analysis depends upon which solution Nature has chosen.

Table VI compares the sensitivity of Super-Kamiokande and SNO to the earth regeneration effect for three different statistical tests. We have computed the number of standard deviations by which the best-fit MSW solutions (described in Sec. IV) differ from the undistorted zenith-angle exposure function. We consider the first and second moments of the zenith-angle distribution (see Section V), the day-night asymmetry (A_{n-d}) (see Sec. VI), and the Kolmogorov-Smirnov test of the distorted zenith-angle distribution. We assume 30000 events are detected in the case of the SMA solution. The comparison is made after only 5000 events are observed for the more-easily recognized LMA solution.

For the SMA solution, the moments analysis is most sensitive. The difference for SNO, between 4.9σ (day-night analysis) and 6.5σ (moments distribution), corresponds to 20000

events, or approximately 7 years of data taking. All three statistical tests can easily reveal the best-fit LMA solution, although the day-night asymmetry is the most efficient characterization in this case. The Kolmogorov-Smirnov test is the least sensitive to the SMA solution, but performs better than the moments method for the LMA solution.

We can understand physically why the SMA distortion is most easily detected by measuring the moments while the LMA distortion is most prominent in the day-night asymmetry. Figure 11 shows for Super-Kamiokande the fractional distortion, $[f(\alpha) - Y(\alpha)]/Y(\alpha)$, of the zenith-angle distribution for the best-fit SMA and LMA solutions. One can crudely approximate the distortions by, for the SMA solution, a delta-function near the maximum allowed zenith angle and, for the LMA solution, a step function near $\pi/2$. With these simple approximations, one can show analytically that the first moment and the day-night asymmetry have similar statistical power for the SMA solution, and the second moment is more discriminatory than either the first moment or the day-night asymmetry. The reason that the second moment is so useful for the SMA solution is that in this case the distortion mostly arises when the neutrinos pass through the core at large zenith angles. Because the vacuum mixing angle is small, the enhanced mixing $[\rho_{\text{res}} = 7 \text{ g cm}^{-3}(E/10 \text{ MeV})]$ due to the earth matter effect is particularly significant when the neutrinos traverse the core. Since the vacuum mixing angle is large for the LMA, the matter enhancement is not especially significant in this case and the main regeneration for the LMA solution is due to oscillations that occur in the mantle, i.e., whenever $\alpha > \pi/2$. The day-night asymmetry is well-tuned to this distortion since $A_{\text{n-d}}$ compares the average event rate for $\alpha > \pi/2$ with the event rate for $\alpha < \pi/2$. The LOW solution produces a relative distortion, $[f(\alpha) - Y(\alpha)]/Y(\alpha)$, that has a shape similar to the LMA solution and is therefore most easily detected by the day-night asymmetry. The Kolmogorov-Smirnov test is not optimally tuned to any of the three best MSW solutions and is therefore not as powerful as the moments or the day-night asymmetry.

IX. MOMENTS OF THE ENERGY SPECTRUM

We refine in this section our previous calculations of the first two moments of the energy spectrum from electron recoils produced by interactions with ${}^8\text{B}$ neutrinos. We use here the slightly improved MSW solutions, described in Sec. IV, that include regeneration in the earth. The reader is referred to our earlier paper [50] for the relevant definitions and notation (see also ref. [34] for a similar calculation).

Table VII presents, for an assumed threshold of 5 MeV, the first and second moments of the electron recoil energy spectrum, and the percentage shifts with respect to the average electron kinetic energy, T_0 , and the dispersion in the kinetic energy, σ_0 , in the absence of oscillations. The results for T_0 and σ_0 differ by small amounts ($< 1\%$) from our earlier results given in ref. [50]; the present results are numerically more precise. The results in Table VII are given for the best-estimate MSW solutions (SMA, LMA, and LOW) described in Sec. IV. For completeness, we list the one year average moments of the energy spectrum for day-time, night-time, and the total year. The calculated moments for the Super-Kamiokande experiment are given in the upper part of the table and the moments for SNO are listed in the lower part of the table. Table VIII presents the same results for an assumed threshold of 6 MeV.

We did not include in our calculation the unknown trigger efficiencies of Super-Kamiokande or SNO. The inclusion of these trigger functions can change the predicted first and second moments of the energy distribution by a few percent and will certainly be included in the careful Monte Carlo calculations that will be performed ultimately by the Super-Kamiokande and SNO experimental groups.

Comparing the calculated day and night rates, Table VII and Table VIII show that regeneration in the earth slightly decreases, for both the SMA and the LOW solutions, the average kinetic energy of the recoil electrons in both Super-Kamiokande and SNO. This decrease occurs because in the sun these two solutions preferentially transform low energy neutrinos from ν_e to ν_μ (or ν_τ) and therefore there is a relatively larger chance at low energy

of regenerating ν_e from ν_μ (or ν_τ) in the earth. For the LMA solution, regeneration increases the average kinetic energy since in this case the high-energy part of the ^8B neutrino energy spectrum is preferentially depleted of ν_e in the sun.

The shift between day and night of the moments is most significant for the LMA solution. In fact, if the nature has chosen the LMA solution, then the spectral distortion may be highlighted by comparing the day-time and night-time moments.

X. SENSITIVITY TO EARTH MODELS AND SOLAR MODELS

We calculate in Sec. X A the sensitivity of the MSW predictions to the assumed density profile and chemical composition of the earth model and in Sec. X B the dependence upon the assumed model of the sun.

A. Uncertainties Due to Earth Models

Table I presents the calculated percentage shifts of the first two moments of the zenith-angle event distribution for all six models of the earth discussed in Sec. III; the calculations were made assuming either the SMA or the LMA solutions. The fractional changes of the first moment vary by only $\sim 0.02\%$ for the SMA solution and $\sim 0.2\%$ for the LMA solution, although the density profiles in some of these models are significantly different from the range allowed by current seismological data. We conclude that the shape of the zenith-angle distribution can be calculated with acceptable accuracy for any of the recently published density profiles of the earth.

Table IX illustrates the uncertainties in the MSW predictions of the shifts of the first and second moments of the zenith-angle distribution due to uncertainties in the electron number density in the mantle and in the core. The ranges of Z/A included in the table ($\pm 2\%$ in the core and -1% , -2% in the mantle) are larger than the current estimates of the geophysical uncertainties (see the discussion in Sec. III and reference [44,45]). We conclude

from Table IX that uncertainties in the chemical composition affect the predicted moment shifts due to regeneration by at most a few percent of their values.

A simplified model with a uniform composition of $Z/A = 0.5$ has been used in reference [35] (and in many or most of the early calculations related to the regeneration effect, see [13]). The predictions from this constant-composition model are also given in Table IX; this crude model leads to imprecise, but not grossly erroneous, predictions of the moments of the zenith-angle distribution.

B. Uncertainties Due to Solar Models

To the best of our knowledge, all previous discussions of the earth regeneration effect have described this phenomenon as if it were completely independent of solar models. This implicit assumption is not exactly correct since the size of the earth regeneration effect depends upon the flavor content of the incident neutrino beam, which must be calculated by using a solar model to describe (for specified MSW parameters) the production and conversion probabilities of ^8B solar neutrinos as a function of the position in the sun at which the neutrinos are created and the neutrino energy. The slightly different density distributions in different solar models have the largest effect, which is still quite small as we shall see below, on the inferred flavor content of the incident solar neutrino flux.

In order to quantify the dependence of the predicted earth regeneration effect upon the characteristics of the solar model, we have calculated the fractional shifts of the first and second moments of the zenith-angle event distribution using three different solar models. As our standard solar model, we adopt the model with helium and heavy element diffusion of Bahcall and Pinsonneault [6]. For comparison, we use the 1992 model of Bahcall and Pinsonneault [52], which includes helium diffusion (but not heavy element diffusion) and somewhat less accurate input physics. Finally, we use the 1988 model of Bahcall and Ulrich [53], which does not include any diffusion and has less precise opacities, equation of state, and other input data.

Table IV shows that the MSW predictions are essentially identical for the 1992 solar model with helium diffusion and the 1995 solar model with helium and heavy element diffusion plus improved input data. The 1988 solar model leads to predictions that can differ by as much as 10% for the SMA moments that will be measured by SNO. However, this 1988 model is inconsistent with recent helioseismological measurements since the 1988 model does not include diffusion [7].

We conclude that predictions of the earth regeneration effect are practically independent of solar models as long as the models include diffusion (i.e., are consistent with helioseismology).

XI. FUTURE EXPERIMENTS AT THE EQUATOR

Recently Gelb, Kwong and Rosen [28] suggested building a new detector similar to SNO close to the equator in order to increase the sensitivity of the experiment to the earth regeneration effect. An equatorial location maximizes the time neutrinos pass through the core of the earth during one calendar year.

In this section, we calculate the size of the regeneration effect for hypothetical equatorial detectors and compare with the sensitivity of the detectors in their actual positions. We consider equatorial analogues of the Super-Kamiokande, SNO, BOREXINO, and HERON/HELLAZ detectors.

Figure 12 shows the predicted zenith-angle distribution for detectors at the equator. The curve in the upper left panel is the zenith-angle exposure function. The other five panels show the distortion due to regeneration for equatorial analogues of Super-Kamiokande, SNO, ICARUS, BOREXINO, and HERON/HELLAZ. For each detector, only the predicted angular distribution functions are shown for the best-fit solutions to which the relevant detector is sensitive: SMA and LMA for the high-energy boron neutrino detectors (Super-Kamiokande, SNO and ICARUS) and LOW for the low-energy neutrino detectors (BOREXINO and HERON/HELLAZ).

Figure 13 shows the iso-sigma ellipses for the four equatorial detectors. BOREXINO and HERON/HELLAX would be more sensitive to the LOW solution if these detectors were built at the equator. However, the high-energy neutrino detectors (Super-Kamiokande, SNO, and ICARUS) would remain insensitive to the LOW solution even if they were moved to the equator. Low-energy neutrino detectors (BOREXINO and HERON/HELLAZ) also remain insensitive to the SMA and LMA solutions even at the equator.

Table X shows the gain in sensitivity that would occur if detectors like Super-Kamiokande and SNO were built at the equator. The enhancement is represented in the table by the shift in the first and second moment of the zenith-angle distribution and by the day-night asymmetry. The enhancements would be important for the best-fit SMA solution, but less significant for the LMA solution. However, regions of parameter space in the LMA solution for which the predicted shifts in the first and second moments are small could be probed more precisely with detectors at the equator.

XII. DISCUSSION AND CONCLUSIONS

The conversion in the earth of ν_μ (or ν_τ) to the more easily detected ν_e is a distinctive prediction of the MSW effect that offers the possibility of unambiguously establishing the existence of physics beyond the standard electroweak model. Because of the importance of this subject, we have carried out precise numerical calculations of the size of the regeneration effect predicted by different MSW parameters that are consistent with the experimental results from the chlorine, Kamiokande, GALLEX, and SAGE experiments. Our results show the potential of the new experiments, Super-Kamiokande, SNO, ICARUS, BOREXINO, HERON, and HELLAZ, for discovering the regeneration effect.

Our results provide the most precise predictions available of the expected zenith-angle distribution of the solar neutrino events in the absence of new physics and in the presence of MSW distortions. The results are obtained by numerical calculations that are discussed in Sec. V and illustrated in Fig. 5 (for Super-Kamiokande and SNO) and Fig. 6 (for the Gran

Sasso experiments ICARUS, BOREXINO, and HERON/HELLAZ).

We present the predictions for the small mixing angle (SMA), large mixing angle(LMA), and low mass (low probability, LOW) MSW solutions of the solar neutrino problems. The parameters of these MSW solutions, which are consistent with the results of the chlorine, Kamiokande, GALLEX, and SAGE experiments, are given in Sec. IV. Our solutions include self-consistently the effects of earth regeneration.

Figure 3 shows the allowed regions of the three MSW solutions in the $\Delta m^2 - \sin^2 2\theta$ plane. Figure 4 presents the survival probabilities as a function of energy for ν_e created in the sun. This figure compares survival probabilities computed for the day (without regeneration) with survival probabilities for the night (with regeneration) and with the average annual survival probabilities.

We describe the predicted MSW distortions in terms of the first two moments of the zenith angle distribution of neutrino events (see Sec. VI), as well as in terms of the traditional day-night asymmetry (see Sec. VII). We analyze simulated data in Sec. VIII and show that the moments of the zenith-angle distribution are more sensitive to the harder-to-detect SMA solution. The predicted large effect of the LMA solution is more easily discovered with the conventional day-night asymmetry.

The “bottom line” is illustrated succinctly in Fig. 9. This figure shows that the current best-estimate MSW solutions predict statistically significant deviations from the undistorted zenith-angle moments for the Super-Kamiokande, SNO, and ICARUS experiments (which are sensitive to the SMA and LMA solutions) and the BOREXINO and HERON/HELLAZ experiments (which are sensitive to the LOW solution).

We have considered a number of effects that have not been previously investigated in connection with the earth regeneration effect. We have calculated the sensitivity of the MSW predictions to a wide range of density profiles of the earth and also to a set of extreme chemical compositions. These calculations are discussed in Sec. III and Sec. X A. We also evaluate the slight dependence of the predicted earth regeneration effect upon the assumed solar model used to calculate the flavor content of the incident neutrino beam (see Sec. X B).

Our results show that these usually-neglected effects associated with the earth and solar models are rather small.

For completeness, we have carried out calculations for hypothetical new detectors that might be built near the equator. These calculations are described in Sec. XI and show quantitatively the enhanced sensitivity to the earth regeneration effect of equatorial detectors, as emphasized by Gelb *et al.* [28].

Using the best-fit MSW solutions calculated here that include the earth regeneration effect, we have evaluated the first and second moments of the electron recoil energy spectrum for ^8B neutrinos detected in Super-Kamiokande and SNO. These calculations, summarized in Sec. VI and in Table VII and Table VIII, refine our earlier results [50] (see also ref. [34]) for the moments of the electron recoil spectrum. Perhaps most importantly, they show that for the LMA solution the comparison of the recoil electron energy spectrum between day and night may reveal a distortion that is not apparent in the temporal average of the energy spectrum.

What would we learn from an observation which showed that the neutrino counting rate depended upon solar direction? The experimental demonstration of a dependence of solar neutrino event rate upon the direction of the sun would not only constitute a direct proof of new physics but would at the same time eliminate a number of the popular alternatives to the MSW effect. Many of the alternatives to the MSW effect, such as vacuum oscillations, magnetic moment transitions, and violations of the equivalence principle predict that the counting rate is independent of the zenith angle position of the sun.

ACKNOWLEDGMENTS

This work has been supported by NSF grant #PHY-9513835. We are indebted to M. Fukugita, E. Lisi, and A. Smirnov for valuable comments on the draft manuscript. We are grateful to E. Lisi, W. Press, P. Rosen, and A. Smirnov for stimulating discussions and to D. L. Anderson, P. Goldreich, F. Press, and A. Rubin for valuable communications regarding

seismological models of the earth.

APPENDIX A: NEUTRINO SURVIVAL PROBABILITIES

In order to calculate the event rates as a function of time we first compute, following the prescription in Ref. [54], the electron neutrino survival probabilities, P_{SE} , after traversing the earth. We begin by using the analytical approximation developed in Ref. [55] of the survival probabilities, P_S , for an electron neutrino passing through the sun; these solar survival probabilities are averaged over the relevant neutrino production regions for ${}^8\text{B}$, ${}^7\text{Be}$, pp , pep , and CNO neutrinos. Assuming that the neutrinos arriving at the earth represent an incoherent superposition of mass-eigenstates [56], we calculate the electron neutrino survival probability after passing through the earth, P_{SE} , from the expression:

$$P_{SE} = \frac{P_S - \sin^2 \theta + P_{2e}(1 - 2P_S)}{\cos 2\theta}. \quad (\text{A1})$$

Here θ is the neutrino mixing angle in vacuum and P_S is the probability of an electron neutrino produced in the sun to arrive as an electron neutrino at the earth. The ambiguity in the above equation for maximal mixing ($\cos 2\theta = 0$) is only apparent. It can be shown that in this case both P_S and P_{SE} are equal to $1/2$. The probability P_{2e} to find an electron neutrino after passing through the earth, if the initial state describing a neutrino entering the earth is the pure mass-eigenstate ν_2 , is calculated numerically by integrating the evolution equations for neutrino states in matter in the form given in [57]. A key point in the calculation is that these survival probabilities as a function of $E/\Delta m^2$ need be calculated just once for each $\sin^2 2\theta$ and for a fixed set of trajectories. We have chosen a set of 180 trajectories equally spaced between 90 and 180 degrees of zenith angle separated by 0.5 degrees. This set is the same for each solar neutrino detector since the density profiles used in our calculations and described in Sec. III are spherically symmetric. The survival probabilities along each trajectory, P_{SE}^i , have been calculated for a grid of 201x201 values of $E/\Delta m^2$ and $\sin^2 2\theta$:

$$10^3 \text{ MeV/eV}^2 \leq E/\Delta m^2 \leq 10^{13} \text{ MeV/eV}^2, \quad (\text{A2a})$$

and

$$10^{-4} \leq \sin^2 2\theta \leq 1. \quad (\text{A2b})$$

The numerical precision of the calculated survival probabilities along each trajectory is better than 0.1%.

The one-year averaged survival probability is given by:

$$\bar{P}_{SE} = \sum_{i=1}^N P_{SE}^i Y(\alpha_i), \quad (\text{A3})$$

where the sum is over zenith angles from 0 to 180 degrees. ($N = 360$ in our case). The zenith-angle exposure function is defined in Sec. V. Correspondingly, the one-year averaged night-time survival probability is given by

$$\bar{P}_{SE}^n = \sum_{i=N/2}^N P_{SE}^i Y(\alpha_i), \quad (\text{A4})$$

where the sum now runs over angles from 90 to 180 degrees. Since the night-time and day-time intervals within one year are equal, the day-time event rate is simply

$$\bar{P}_{SE}^d = 0.5 P_{SE}. \quad (\text{A5})$$

With the calculated survival probabilities, it is straightforward to determine the corresponding total event rates, as well as the day-time and night-time one-year averaged event rates in any solar neutrino detector.

APPENDIX B: TIME DEPENDENCE OF THE ZENITH ANGLE

The dependence of the solar zenith angle on the time of the year and on the geographic location of the detectors is given by the following set of formulae [49]:

$$\cos \alpha = \sin \delta \sin \phi + \cos \delta \cos \phi \cos H, \quad (\text{B1a})$$

$$\sin \delta = \sin \epsilon \sin \lambda, \quad (\text{B1b})$$

$$L = 280^{\circ}.461 + 0^{\circ}.9856003n, \quad (\text{B1c})$$

$$n = -1462.5 + D + H, \quad (\text{B1d})$$

$$g = 357^0.528 + 0^0.9856003n, \quad (\text{B1e})$$

and

$$\lambda = L + 1^0.915 \sin g + 0^0.020 \sin 2g. \quad (\text{B1f})$$

The precision in the apparent coordinates of the Sun is $0^0.01$ and the precision of the equation of time is 6 seconds between the years 1950 and 2050. Here H is the fraction of day from 0^h UT, D is day of the year (counting from January 1), n is the number of days from Julian year 2000.0, λ is the ecliptic longitude, L is the mean longitude of the sun (corrected for aberration), $\epsilon = 23^0.439 - 0.0000004n$ is the obliquity of the ecliptic, δ is the sun's declination, and g is the mean anomaly[§].

The distance of the sun from the earth in astronomical units ($1 \text{ AU} = 1.495978706(2) 10^{11}$ m) is given by the formula:

$$R = 1.0014 - 0.01671 \cos g - 0.00014 \cos 2g. \quad (\text{B2})$$

Equation (B2) has been used in the calculation of the day-night asymmetries and the shifts of the first two moments of the zenith-angle distribution.

APPENDIX C: CHARACTERISTICS OF FUTURE DETECTORS

We describe in this Appendix the characteristics we have assumed for Super-Kamiokande [22], SNO [23], ICARUS [24], BOREXINO [25], HERON [26] and HELLAZ [27]. The Super-Kamiokande, SNO and ICARUS detectors are sensitive only to high-energy ^8B neutrinos, while BOREXINO is sensitive primarily to ^7Be neutrinos ($E_\nu = 0.862 \text{ MeV}$) and the HERON and HELLAZ detectors are being designed to detect low energy ($E_\nu < 0.44 \text{ MeV}$) pp neutrinos.

[§]For definitions of these astronomical quantities see Ref. [49]

For the Super-Kamiokande detector, we adopt a threshold of 5 MeV and a trigger efficiency of 50% at this energy [22]. The energy resolution function is assumed to have a gaussian shape with FWHM of 1.6 MeV at electron kinetic energy 10 MeV. We have performed calculations, which show that the sensitivity of our results to the assumed energy resolution and trigger efficiency of the detector.

For the SNO detector, we calculate only the rate of the CC reaction, namely $\nu_e + d \rightarrow p + p + e^-$. We adopt [58] a threshold of 5 MeV and an energy resolution function with a 1σ uncertainty of 1.1 MeV at 10 MeV electron kinetic energy. The CC cross-section for SNO was taken from Ref. [18]. The trigger efficiency function has been approximated with a step function at the threshold of the detector.

Reference [50] gives further details regarding our characterization of SNO and Super-Kamiokande.

For ICARUS, we have considered only the superallowed transition and have used the neutrino absorption cross sections given in ref. [5]. We have assumed a neutrino threshold for detection that corresponds to electrons being produced with at least 5 MeV of energy, which requires a minimum neutrino energy of 10.9 MeV.

The BOREXINO detector is being developed as a neutrino-electron scattering experiment that will measure the flux of ${}^7\text{Be}$ neutrinos, using the step in the energy distribution of neutrino-electron scattering events at the maximum recoil-electron kinetic energy of $T_e = 0.62$ MeV. The detector characteristics that are knowable *a priori* (which does not include the crucial background rate versus energy) are not as important as for SNO and Super-Kamiokande and we need to compute only the ν_e survival probability. We include radiative corrections to the neutrino-electron cross-section, calculated in [59], which for recoil electron energies below 0.62 MeV are less than 1%. The ratio of the $(\nu_\mu e)$ to $(\nu_e e)$ total cross-sections for neutrino energy 0.862 MeV is $\sigma_{\nu_\mu, e}/\sigma_{\nu_e, e} = 0.221$.

HERON and HELLAZ are also neutrino-electron scattering experiments with very different preliminary designs, but with the same target material, helium. They will measure the flux and spectral shape of pp neutrinos. We have assumed a threshold of 0.1 MeV

and a perfect energy resolution (delta function). The trigger efficiency is represented by a step-function at the threshold of the detector. We again use neutrino-electron cross-sections including radiative corrections [59].

The event rate, Q , averaged over certain time interval, τ , in a neutrino-electron-scattering experiment, such as Super-Kamiokande, BOREXINO, HERON or HELLAZ is given by

$$\langle Q \rangle_\tau = \int_0^{E_{\max}} \Phi(E_\nu) \left[Z_{\nu_e}(E_\nu) \langle P(E_\nu) \rangle_\tau + Z_{\nu_\mu}(E_\nu) (1 - \langle P(E_\nu) \rangle_\tau) \right] dE_\nu \quad (\text{C1})$$

Here $Z_{\nu_e(\nu_\mu)}$ are the response functions of the detector to either ν_e or ν_μ , Φ is the solar neutrino flux to which the detector is sensitive, E_ν is the neutrino energy, E_{\max} is the end point of the neutrino energy spectrum and $\langle P \rangle_\tau$ is the average survival probability for the chosen time interval τ . The interval can be, e.g., the total day-time or night-time during one calendar year, or a whole calendar year including both days and nights. The calculation of the average survival probabilities is described in Appendix A (Eqs. A1-A5). The response functions represent the convolution of the absorption cross sections with the detector characteristics (see Ref. [50] for details).

- [1] K. Lande, to be published in *Neutrino 96*, Proceedings of the 17th International Conference on Neutrino Physics and Astrophysics, Helsinki, Finland, 13–19 June 1996, edited by K. Huitu, K. Enqvist, and J. Maalampi (World Scientific, Singapore); see also, R. Davis, *Prog. Part. Nucl. Phys.* **32**, 13 (1994); B. T. Cleveland *et al.*, *Nucl. Phys. B (Proc. Suppl.)* **38**, 47 (1995).
- [2] Y. Fukuda *et al.* (Kamiokande Collaboration), *Phys. Rev. Lett.* **77**, 1683 (1996).
- [3] T. Kirsten *et al.* (GALLEX Collaboration), to be published in *Neutrino 96*, Proceedings of the 17th International Conference on Neutrino Physics and Astrophysics, Helsinki, Finland, 13–19 June 1996, edited by K. Huitu, K. Enqvist, and J. Maalampi (World Scientific, Singapore); for earlier results, see, P. Anselmann *et al.*, *Phys. Lett. B* **327**, 377 (1994); **342**, 440 (1995); **357**, 237 (1995).

- [4] V. Gavrin *et al.* (SAGE Collaboration), in *Neutrino 96*, Proceedings of the 17th International Conference on Neutrino Physics and Astrophysics, Helsinki, Finland, 13–19 June 1996, edited by K. Huitu, K/ Enqvist, and J. Maalampi (World Scientific, Singapore); see also, G. Nico *et al.*, in *Proceedings of the XXVII International Conference on High Energy Physics*, Glasgow, Scotland, 1994, edited by P. J. Bussey and I. G. Knowles (Institute of Physics, Bristol, 1995), p. 965; J. N. Abdurashitov *et al.*, *Phys. Lett. B* **328**, 234 (1994).
- [5] J. N. Bahcall, *Neutrino Astrophysics* (Cambridge University Press, Cambridge, England, 1989).
- [6] J. N. Bahcall and M. H. Pinsonneault, *Rev. Mod. Phys.* **67**, 781 (1995).
- [7] J. N. Bahcall, M. H. Pinsonneault, S. Basu and J. Christensen-Dalsgaard, *Phys. Rev. Lett.* **78**, 171 (1997).
- [8] J. N. Bahcall, R. Davis, Jr., P. Parker, A. Smirnov, and R. Ulrich, eds., *Solar Neutrinos, The First Thirty Years*, *Frontiers in Physics*, Vol. 92 (Addison-Wesley, Reading, MA, 1994).
- [9] J. N. Bahcall, to be published in the Proceedings of the 18th Texas Symposium on Relativistic Astrophysics, December 15–20, 1996, Chicago, Illinois, edited by A. Olinto, J. Frieman, and D. Schramm (World Scientific, Singapore) (hep-ph/9702057).
- [10] K. M. Heeger and R. G. H. Robertson, *Phys. Rev. Lett.* **77**, 3720 (1996).
- [11] J. N. Bahcall and P. I. Krastev, *Phys. Rev. D* **53**, 4211 (1996).
- [12] L. Wolfenstein, *Phys. Rev. D* **17**, 2369 (1978); S. P. Mikheyev and A. Yu. Smirnov, *Yad. Fiz.* **42**, 1441 (1985) [*Sov. J. Nucl. Phys.* **42**, 913 (1985)]; *Nuovo Cimento C* **9**, 17 (1986).
- [13] S. P. Mikheyev and A. Yu. Smirnov, in *'86 Massive Neutrinos in Astrophysics and in Particle Physics*, proceedings of the Sixth Moriond Workshop, edited by O. Fackler and Y. Trân Thanh Vân (Editions Frontières, Gif-sur-Yvette, 1986), p. 355; J. Bouchez *et al.*, *Z. Phys. C* **32**, 499 (1986); M. Cribier, W. Hampel, J. Rich, and D. Vignaud, *Phys. Lett. B* **182**, 89 (1986); M.

- L. Cherry and K. Lande, Phys. Rev. D **36**, 3571 (1987); S. Hiroi, H. Sakuma, T. Yanagida, and M. Yoshimura, Phys. Lett. B **198**, 403 (1987); S. Hiroi, H. Sakuma, T. Yanagida, and M. Yoshimura, Prog. Theor. Phys. **78**, 1428 (1987); A. Dar, A. Mann, Y. Melina, and D. Zajfman, Phys. Rev. D **35**, 3607 (1988); M. Spiro and D. Vignaud, Phys. Lett. B **242**, 279 (1990).
- [14] A. J. Baltz and J. Weneser, Phys. Rev. D **35**, 528 (1987).
- [15] A. J. Baltz and J. Weneser, Phys. Rev. D **37**, 3364 (1988).
- [16] H. Bethe, Phys. Rev. Lett. **56**, 1305 (1986); S. P. Rosen and J. M. Gelb, Phys. Rev. D **34**, 969 (1989); E. W. Kolb, M. S. Turner, and T. P. Walker, Phys. Lett. B **175**, 478 (1986).
- [17] H. H. Chen, Phys. Rev. Lett. **55**, 1534 (1985).
- [18] J. N. Bahcall and E. Lisi, Phys. Rev. D **54**, 5417 (1996).
- [19] V. N. Gribov and B. M. Pontecorvo, Phys. Lett. B **28**, 493 (1969).
- [20] M. B. Volshin, M. I. Vysotsky, and L. B. Okun, Sov. Phys. JETP **64**, 446 (1986).
- [21] M. Gasperini, Phys. Rev. **D38**, 2635 (1988).
- [22] Y. Totsuka, in *TAUP '95*, proceedings of the International Workshop on Theoretical and Phenomenological Aspects of Underground Physics, Toledo, Spain, 17–21 September 1995, edited by A. Morales, J. Morales, and J. A. Villar (North-Holland, Amsterdam, 1996), p. 547 [Nucl. Phys. B (Proc. Suppl.) **48**, 1996]; A. Suzuki, in *Physics and Astrophysics of Neutrinos*, edited by M. Fukugita and A. Suzuki (Springer Verlag, Tokyo, 1994) p. 414.
- [23] G. T. Ewan *et al.* (SNO Collaboration), Sudbury Neutrino Observatory Proposal, Report No. SNO-87-12, 1987 (unpublished); Scientific and Technical Description of the Mark II SNO Detector, edited by E. W. Beier and D. Sinclair, Queen's University Report No. SNO-89-15, 1989 (unpublished); A. B. McDonald, in *Particle Physics and Cosmology*, proceedings of the 9th Lake Louise Winter Institute, edited by A. Astbury *et al.* (World Scientific, Singapore, 1995), p. 1.

- [24] A First 600 Ton ICARUS Detector Installed at the Gran Sasso Laboratory, addendum to proposal LNGS-94/99 I and II, Report No. LNGS-95/10, 1995 (unpublished); J. N. Bahcall, M. Baldo-Ceolin, D. Cline, and C. Rubbia, *Phys. Lett. B* **178**, 324 (1986).
- [25] C. Arpesella *et al.*, BOREXINO proposal, Vols. 1 and 2, edited by G. Bellini *et al.* (Univ. of Milano, Milano, 1992); R. S. Raghavan, *Science* **267**, 45 (1995).
- [26] R. E. Lanou, H. J. Maris, and G. M. Seidel, *Phys. Rev. Lett.* **58**, 2498 (1987); S. R. Bandler *et al.*, *J. Low Temp. Phys.* **93**, 785 (1993); The HERON collaboration, *Phys. Rev. Lett.* **68**, 2429 (1992); *Rev. Sci. Instrum.* **63**, 230 (1992); *Phys. Lett. B* **341**, 431 (1995); *Phys. Rev. Lett.* **74**, 3169 (1995).
- [27] G. Laurenti *et al.*, in *Proceedings of the Fifth International Workshop on Neutrino Telescopes, Venice, Italy, 1993*, edited by M. Baldo-Ceolin (Padua Univ., Padua, Italy, 1994), p. 161; G. Bonvicini, *Nucl. Phys. B* **35**, 438 (1994).
- [28] J. M. Gelb, W. Kwong, and S. P. Rosen, *Phys. Rev. Lett.* **78**, 2296 (1997).
- [29] R. Davis and K. Lande (private communication); see also the paper by Cherry and Lande in ref. [13].
- [30] K. S. Hirata *et al.*, *Phys. Rev. Lett.* **65**, 1301 (1990).
- [31] A. J. Baltz and J. Weneser, *Phys. Rev. D* **50**, 5971 (1994); **51**, 3960 (1995).
- [32] N. Hata and P. Langacker, *Phys. Rev. D* **48**, 2937 (1993); *Phys. Rev. D* **50**, 632 (1994).
- [33] P. I. Krastev, talk at the DPF '96 meeting, August 1996, Minneapolis, Minnesota (to be published in the Proceedings), hep-ph/9610339.
- [34] E. Lisi and D. Montanino, preprint BARI-TH-260-97, hep-ph/9702343, *Phys. Rev. D* (August 1, 1997).
- [35] Q. Y. Liu, M. Maris, and S. T. Petcov, preprint SISSA-16-97-EP, hep-ph/9702361; M. Maris and S. T. Petcov, hep-ph/9703207.

- [36] V. N. Zharkov, *Interior Structure of the Earth and Planets* (Harwood Academic Publishers, New York, 1986).
- [37] A. M. Dziewonski and D. L. Anderson, *Phys. Earth Planet. Interior* **25**, 207 (1981).
- [38] K. E. Bullen, *The Earth's Density* (Chapman and Hall, London, 1975).
- [39] F. D. Stacey, *Physics of the Earth* (John Wiley and Sons, New York, 1969).
- [40] K. E. Bullen, *The Earth's Density* (Chapman and Hall, London, 1975), p. 359.
- [41] A. M. Dziewonski and F. Gilbert, *Geophys. J. R. Astron. Soc.* **35**, 401 (1973).
- [42] T. H. Jordan and D. L. Anderson, *Geophys. J. R. Astron. Soc.* **36**, 411 (1974).
- [43] K. E. Bullen and R. A. Haddon, *Proc. Nat. Acad. Sci. Wash.* **58**, 846 (1967).
- [44] W. A. Anderson and Th. J. Ahrens, *J. Geophys. Res.* **99**, 4273 (1994); E. Kittle and R. Jeanholz, *J. Geophys. Res.* **96**, 16169 (1991); R. Jeanholz, *Annu. Rev. Earth Planet. Sci.* **18**, 357 (1990).
- [45] Y. Zhao and D. L. Anderson, *Phys. Earth Planet. Interior*, **85**, 273 (1994).
- [46] K. S. Hirata *et al.*, *Phys. Rev. D* **44**, 2241 (1991); see also Ref. [2].
- [47] G. L. Fogli and E. Lisi, *Astropart. Phys.* **3**, 185 (1995).
- [48] P. I. Krastev and S. T. Petcov, *Phys. Lett. B* **299**, 99 (1993); G. L. Fogli, E. Lisi, and D. Montanino, *Phys. Rev. D* **54**, 2048 (1996).
- [49] *The Astronomical Almanac, 1996* (U.S. Government Printing Office, Washington).
- [50] J. N. Bahcall, P. I. Krastev, and E. Lisi, *Phys. Rev. C* **55**, 494 (1997).
- [51] M. G. Kendall and A. Stuart, *The Advanced Theory of Statistics* (Hafner, New York, 1969), Vol. I.
- [52] J. N. Bahcall and M. H. Pinsonneault, *Rev. Mod. Phys.* **64**, 885 (1992).

- [53] J. N. Bahcall and R. K. Ulrich, *Rev. Mod. Phys.* **60**, 297 (1988).
- [54] S. P. Mikheyev and A. Yu. Smirnov, in *New and Exotic Phenomena*, proceedings of the Seventh Moriond Workshop, edited by O. Fackler and Y. Trân Thanh Vân (Editions Frontières, Gif-sur-Yvette, 1987), p. 403.
- [55] P. I. Krastev and S. T. Petcov, *Phys. Lett. B* **207**, 64 (1988).
- [56] S. P. Mikheyev and A. Yu. Smirnov, *Usp. Fiz. Nauk* **153**, 3 (1987) [*Sov. Phys.–Usp.* **30**, 759 (1987)]; *Prog. Part. Nucl. Phys.* **23**, 41 (1988).
- [57] S. P. Mikheyev and A. Yu. Smirnov, *Nuovo Cimento* **9C**, 17 (1986).
- [58] E. W. Beier (private communication).
- [59] J. N. Bahcall, M. Kamionkowski, and A. Sirlin, *Phys. Rev. D* **51**, 6146 (1995).
- [60] D. L. Anderson, *Theory of the Earth*, (Blackwell Scientific Publications, 1989).

TABLE I. Sensitivity to the model of the earth. The table illustrates the weak dependence on the model of the earth of the calculated changes in the first and second moments of the angular distribution of events in the Super-Kamiokande and SNO detectors. The density distributions in the six models of the earth listed in the table span a range of possibilities that is much larger than suggested by current geophysical knowledge. The second and third columns give the total mass, M_{\oplus} (in 10^{27} g), and the moment of inertia, I (in 10^{45} gcm²), for each model. The mass of the earth is 5.97370 ± 0.00076 , the polar value of the moment of inertia is 0.804, and the equatorial value is 0.801 [60].] The last four columns give the fractional shift in percent of the first two moments ($\Delta\alpha/\alpha_0$ and $\Delta\sigma^2/\sigma_0^2$) of the zenith-angle distribution of events in the Super-Kamiokande and SNO detectors for the SMA (upper entry) and for the LMA (lower entry) solutions.

			$\Delta\langle\alpha\rangle/\alpha_0$	$\Delta\sigma^2/\sigma_0^2$	$\Delta\langle\alpha\rangle/\alpha_0$	$\Delta\sigma^2/\sigma_0^2$
Model	M_{\oplus}	I	Super-Kamiokande (%)	Super-Kamiokande (%)	SNO (%)	SNO (%)
PREM	5.972	0.802	1.02	2.03	1.04	2.42

1981			3.23	-0.33	5.28	-2.20
HB' ₁	5.970	0.801	1.00	2.00	1.02	2.38
1975			3.29	-0.27	5.37	-2.09
B497	5.067	0.800	1.01	2.03	1.03	2.41
1973			3.22	-0.26	5.26	-2.05
B1	5.949	0.798	1.01	2.03	1.03	2.42
1974			3.23	-0.33	5.21	-2.38
A''	5.946	0.798	1.00	2.01	1.01	2.39
1967			3.29	-0.51	5.35	-2.55
Stacey	5.973	0.802	1.00	2.01	1.02	2.38
1969			3.27	-0.28	5.34	-2.11

TABLE II. Solar neutrino data used in the analysis. The experimental results are given in SNU for all of the experiments except Kamiokande, for which the result is expressed as the measured ^8B flux above 7.5 MeV in units of $\text{cm}^{-2}\text{s}^{-1}$ at the earth. The ratios of the measured values to the corresponding predictions in the standard solar model of Ref. [6] are also given. The result cited for the Kamiokande experiment assumes that the shape of the ^8B neutrino spectrum is not affected by physics beyond the standard electroweak model.

Experiment	Result	Theory	Units	Result/Theory	Reference
HOMESTAKE	$2.56 \pm 0.16 \pm 0.14$	$9.5^{+1.2}_{-1.4}$	SNU	0.27 ± 0.022	[1]
KAMIOKANDE	$2.80 \pm 0.19 \pm 0.35$	$6.62^{+0.93}_{-1.12}$	$10^6 \text{ cm}^{-2} \text{ s}^{-1}$	0.42 ± 0.060	[2]
GALLEX	$69.7 \pm 6.7 \pm^{+3.9}_{-4.5}$	136.8^{+8}_{-7}	SNU	0.51 ± 0.058	[3]
SAGE	$72^{+12}_{-10} \ ^{+5}_{-7}$	136.8^{+8}_{-7}	SNU	0.53 ± 0.095	[4]

TABLE III. Northern latitudes (in degrees) for several solar neutrino detectors. These angles correspond to ϕ in Fig. 1.

Homestake	Kamioka	Gran Sasso	Baksan	Sudbury
44.3	36.4	42.4	43.3	46.3

TABLE IV. Sensitivity to Solar Models. Values of the percentage shifts of the first and second moments of the zenith-angle event distribution in Super-Kamiokande and SNO computed with three different solar models (BU1988, BP1992, BP1995).

Detector	Solar Model	SMA		LMA	
		$\Delta\langle\alpha\rangle/\alpha_0$	$\Delta\sigma^2/\sigma_0^2$	$\Delta\langle\alpha\rangle/\alpha_0$	$\Delta\sigma^2/\sigma_0^2$
Super-Kamiokande	1995	1.02	2.03	3.22	-0.32
	1992	1.02	2.03	3.22	-0.32
	1988	0.96	1.94	3.22	-0.32
SNO	1995	1.04	2.42	5.28	-2.20
	1992	1.04	2.44	5.28	-2.20
	1988	0.96	2.26	5.27	-2.20

TABLE V. Day-night asymmetry in Super-Kamiokande and SNO. The table gives the magnitude of the expected day-night asymmetry (A_{n-d} , see Eq. (9)) (in percent) in Super-Kamiokande and SNO for values of the neutrino oscillation parameters Δm^2 and $\sin^2 2\theta$ corresponding to the best-fit SMA and LMA solutions (see Eqs. 1a,1b and 2a,2b). The indicated uncertainties describe the expected limits at 95% C.L.

Solution	Super-Kamiokande	SNO
SMA	1.8 $^{+4.2}_{-2.0}$	2 $^{+6.0}_{-2.4}$
LMA	7.8 $^{+1.4}_{-6.6}$	15 $^{+29}_{-13}$

TABLE VI. What statistical test is best? The table compares the statistical power of three methods for analyzing data on the regeneration effect: a) moments of the zenith-angle distribution, b) day-night asymmetry (A_{n-d}), and c) Kolmogorov Smirnov (K-S) test of the zenith-angle distribution. The number of sigmas listed in the table corresponds to the deviation of the best-fit MSW solutions described in Sec. IV from the undistorted zenith-angle distribution. The numerical results correspond to 30000 events for the SMA solution and 5000 events for the LMA solution.

Detector	Solution	Moments (σ)	A_{n-d} (σ)	K-S test (σ)
Super-Kamiokande	SMA	5	4.4	3.7
	LMA	5.5	9.2	6.3
SNO	SMA	6.5	4.9	4.4
	LMA	10	18.8	12.4

TABLE VII. Moments of the Energy Spectrum. The moments in the absence of oscillations are $T_0 = 7.293$ MeV and $\sigma_0^2 = 3.391$ MeV² for Super-Kamiokande and $T_0 = 7.646$ MeV and $\sigma_0^2 = 3.032$ MeV² for SNO.

MSW Solution		$\langle T \rangle$	$(T - T_0)/T_0$	σ^2	$(\sigma^2 - \sigma_0^2)/\sigma_0^2$
		(MeV)	(%)	(MeV ²)	(%)
<u>Super-Kamiokande</u>					
	Day	7.408	1.58	3.591	5.88
SMA	Night	7.403	1.50	3.574	5.38
	Average	7.405	1.54	3.582	5.64
	Day	7.275	-0.25	3.368	-0.67
LMA	Night	7.310	0.23	3.439	1.42
	Average	7.294	0.008	3.408	0.48
	Day	7.298	0.06	3.411	0.58
LOW	Night	7.290	-0.04	3.398	0.20
	Average	7.294	0.008	3.404	0.38
<u>SNO</u>					
	Day	7.869	2.91	3.161	4.25
SMA	Night	7.846	2.62	3.144	3.68
	Average	7.858	2.76	3.152	3.96
	Day	7.644	-0.03	3.032	-0.03
LMA	Night	7.719	0.95	3.113	2.66
	Average	7.687	0.53	3.084	1.72
	Day	7.682	0.47	3.069	1.22
LOW	Night	7.668	0.28	3.060	0.90
	Average	7.675	0.37	3.064	1.06

TABLE VIII. Moments of the Energy Spectrum. The moments in the absence of oscillations are $T_0 = 8.057$ MeV and $\sigma_0^2 = 2.825$ MeV² for Super-Kamiokande and $T_0 = 8.178$ MeV and $\sigma_0^2 = 2.348$ MeV² for SNO.

MSW Solution		$\langle T \rangle$	$(T - T_0)/T_0$	σ^2	$(\sigma^2 - \sigma_0^2)/\sigma_0^2$
		(MeV)	(%)	(MeV ²)	(%)
<u>Super-Kamiokande</u>					
	Day	8.149	1.14	2.968	5.07
SMA	Night	8.143	1.06	2.954	4.56
	Average	8.146	1.10	2.962	4.84
	Day	8.046	-0.14	2.804	-0.76
LMA	Night	8.074	0.22	2.861	1.25
	Average	8.061	0.05	2.833	0.28
	Day	8.064	0.08	2.836	0.40
LOW	Night	8.058	0.01	2.827	0.048
	Average	8.061	0.046	2.832	0.24
<u>SNO</u>					
	Day	8.332	1.88	2.467	5.05
SMA	Night	8.315	1.67	2.452	4.41
	Average	8.323	1.77	2.459	4.72
	Day	8.177	-0.043	2.347	-0.043
LMA	Night	8.239	2.63	2.410	2.63
	Average	8.212	1.84	2.392	1.84
	Day	8.206	0.34	2.379	1.28
LOW	Night	8.196	0.22	2.370	0.94
	Average	8.201	0.28	2.374	1.11

TABLE IX. Dependence of moments on assumed chemical composition. The table gives the relative shifts (in percent) of the first and second moments ($\Delta\mu_i/\mu_i$) of the zenith-angle distribution in Super-Kamiokande and SNO as a function of the assumed chemical composition. The ratio Z/A in the core has been varied by $\pm 0.5\%$, $\pm 1\%$, $\pm 2\%$ (see second column) from the central value $[(Z/A)_{\text{core}} = 0.465]$ adopted in the rest of the paper. The ratio in the mantle has been varied by -1% , -2% from the standard value of $[(Z/A)_{\text{mantle}} = 0.496]$. The last row for each detector corresponds to a simplified model with $Z/A = 0.5$ both in the mantle and in the core. The four columns for each detector correspond to the first and second moment in the SMA and LMA best-fit solutions respectively.

Detector	$\Delta(Z/A)/(Z/A)$ (%)	SMA		LMA	
		$\Delta\langle\alpha\rangle/\alpha_0$ (%)	$\Delta\sigma^2/\sigma_0^2$ (%)	$\Delta\langle\alpha\rangle/\alpha_0$ (%)	$\Delta\sigma^2/\sigma_0^2$ (%)
Super-Kamiokande (core)	-2	1.03	2.06	3.22	-0.338
	-1	1.02	2.05	3.22	-0.329
	-0.5	1.02	2.04	3.22	-0.325
	0.0	1.02	2.03	3.23	-0.323
	+0.5	1.02	2.02	3.23	-0.316
	+1	1.01	2.01	3.23	-0.311
mantle	+2	1.01	1.99	3.23	-0.301
	-1	1.01	2.03	3.19	-0.336
	-2	1.00	2.04	3.16	-0.358
Z/A = 0.5	0	0.98	1.89	3.27	-0.257
SNO	-2	1.05	2.46	5.27	-2.23
	-1	1.04	2.44	5.27	-2.22
	-0.5	1.04	2.43	5.27	-2.21
	0.0	1.04	2.42	5.28	-2.20
	+0.5	1.04	2.41	5.28	-2.20

	+1	1.03	2.40	5.28	-2.19
	+2	1.03	2.38	5.29	-2.17
	-1	1.01	2.38	5.23	-2.15
mantle	-2	0.98	2.33	5.18	-2.10
Z/A = 0.5	0	1.01	2.28	5.33	-2.11

TABLE X. Equatorial enhancement. The magnitude of the regeneration effect is compared for detectors located at their actual positions and at the equator. The size of the effect is represented by the number of standard deviations the first and second moments of the angular distribution differ from the undistorted exposure function (and, in parentheses, the day-night asymmetry in percent). The values of the neutrino oscillation parameters Δm^2 and $\sin^2 2\theta$ correspond to the best-fit SMA and LMA solutions (see Eqs. 1a,1b and 2a,2b). For comparison, the best-fit SMA and LMA solutions produce 5σ and 13σ effects at the actual location of Super-Kamiokande and 6.5σ and 25σ at the actual location of SNO.

Location	Solution	Super-Kamiokande	SNO
Equator	SMA	8σ (3.0 $^{+5.0}_{-3.0}$ %)	9σ (4.1 $^{+7.9}_{-4.1}$ %)
	LMA	14.5σ (7.6 $^{+14}_{-6.3}$ %)	29σ (15 $^{+24}_{-13}$ %)

FIG. 1. Schematic view of detector's location and sun's direction. The zenith is defined as the line from the center of the Earth through the center of the detector. The zenith angle, α , and the latitude of the detector's location, ϕ , are also shown in the figure.

FIG. 2. Density profiles for six different models of the earth. The models are: 1) PREM [37], 2) Stacey's model [39], 3) model HA [43], 4) model HB1' [40], 5) model B497 [41], and 6) model B1 [42]. The radius is given in kilometers from the center of the earth. All models are spherically symmetric.

FIG. 3. Allowed MSW solutions with regeneration. The allowed regions are shown for the neutrino oscillation parameters Δm^2 and $\sin^2 2\theta$. The C.L. for the outer regions is 99% and the C. L for the inner regions is 99% (only applies to the LMA and SMA solutions). The data used here are from the chlorine [1], Kamiokande [2], GALLEX [3], and SAGE [4] experiments. The solar model used is the best standard model of Bahcall and Pinsonneault (1995) with helium and heavy element diffusion [6]. The points where χ^2 has a local minimum are indicated by a circle.

FIG. 4. Survival probabilities for MSW solutions. The figure presents the survival probabilities for a ν_e created in the sun to remain a ν_e upon arrival at the Super-Kamiokande detector. The best-fit MSW solutions including regeneration in the earth are described in Sec. IV. The full line refers to the average survival probabilities computed taking into account regeneration in the earth and the dotted line refers to calculations for the day-time that do not include regeneration. The dashed line includes regeneration at night. There are only slight differences between the computed regeneration probabilities for the detectors located at the positions of Super-Kamiokande, SNO and the Gran Sasso Underground Laboratory.

FIG. 5. Super-Kamiokande and SNO zenith-angle distributions. The figure shows the expected zenith-angle distribution of neutrino events during one calendar year in the Super-Kamiokande and the SNO detectors. The angle, α , represents the angular separation between the direction to the sun and the direction of the local zenith (see Fig. 1). The two left panels display the zenith-angle exposure functions, the undistorted angular distributions in the absence of oscillations. The exposure functions are determined by the location of the two detectors at, respectively, Kamioka, Japan, and Sudbury, Canada. The distorted zenith-angle distributions due to the regeneration effect in the Earth are shown in the two right panels; the neutrino solutions are indicated by: SMA (solid line) and LMA (dotted line).

FIG. 6. Gran Sasso zenith-angle distributions. The figure shows the expected zenith-angle distribution of events during one calendar year in detectors located at the Gran Sasso Laboratory in Italy: ICARUS, BOREXINO, HERON and HELLAZ. The upper left panel shows the zenith-angle exposure function, which does not depend on detector characteristics. The three additional panels display the distorted zenith-angle distributions due to the regeneration effect in the Earth; the solutions are indicated by: SMA (solid line), LMA (dotted line) and LOW (dashed line).

FIG. 7. Contours of constant relative shift (in percent) of the average zenith angle, $(\langle\alpha\rangle - \alpha_0)/\alpha_0$, due to ν_e regeneration in the earth as a function of the neutrino oscillation parameters, $\sin^2 2\theta$ and Δm^2 . Here $\alpha_0 = 90^\circ$ is the average angle of the undistorted angular distribution with no oscillations. The shaded regions in the panels for Super-Kamiokande and SNO are allowed by the latest solar neutrino data at 95% C.L. and represent the SMA and LMA solutions. In the lower two panels (BOREXINO and HERON/HELLAZ) the three shaded regions are allowed at 99% C.L., the low-mass region representing the LOW solution (see text for details). The black circle within each allowed region represents the point which corresponds (locally) to the best-fit to the data.

FIG. 8. Contours of constant relative shift (in percent) of the dispersion of the zenith angle, $(\sigma^2 - \sigma_0^2)/\sigma_0^2$, due to ν_e regeneration in the earth as a function of the neutrino oscillation parameters, $\sin^2 2\theta$ and Δm^2 . The values of σ_0^2 are given in the text for each of the experiments. The definition of the shaded regions is the same as in Fig. 7.

FIG. 9. How many sigmas? The figure shows the sensitivity of Super-Kamiokande, SNO, ICARUS, BOREXINO and HERON/HELLAZ to the regeneration effect. Iso-sigma contours, statistical errors only, delineate the fractional percentage shifts of the first two moments of the angular distribution of events for an assumed 30000 observed events. For all but the ICARUS experiment, the best-fit MSW solutions are indicated by black circles (SMA), squares (LMA), and triangles (LOW); the best-fit solutions are presented in Sec. IV. The error bars on the predicted moments correspond to Δm^2 and $\sin^2 2\theta$ within allowed solution space at 95% C.L. (for Super-Kamiokande, SNO, and ICARUS) or 99% C.L. (BOREXINO and HERON/HELLAZ). For ICARUS, we have indicated the best-fit solutions by a transparent circle, square, or triangle. The best-fit SMA and LOW solutions for ICARUS and the LOW solution for SNO are all three close together at about 3σ from the no oscillation solution. In order to avoid too much crowding in the figure, we have not shown the theoretical uncertainties for ICARUS.

FIG. 10. Contours of constant day-night asymmetry, A_{n-d} (see Eq. (9)), in Super-Kamiokande, SNO, ICARUS, BOREXINO and HERON/HELLAZ. The shaded regions are the same as in Fig. 7.

FIG. 11. Relative distortion for Super-Kamiokande. The figure shows the fractional distortion, $[f(\alpha) - Y(\alpha)]/Y(\alpha)$, of the zenith-angle distribution for the best-estimate SMA and LMA MSW solutions.

FIG. 12. The zenith-angle distribution for equatorial detectors with the characteristics of Super-Kamiokande, SNO, ICARUS, BOREXINO and HERON/HELLAZ. Notation is the same as in Figs. 5 and 6.

FIG. 13. How many sigmas at the equator? The figure shows the sensitivity to the regeneration effect of equatorial detectors with the characteristics of Super-Kamiokande, SNO, ICARUS, BOREXINO and HERON/HELLAZ. Notation is the same as in Fig. 9.

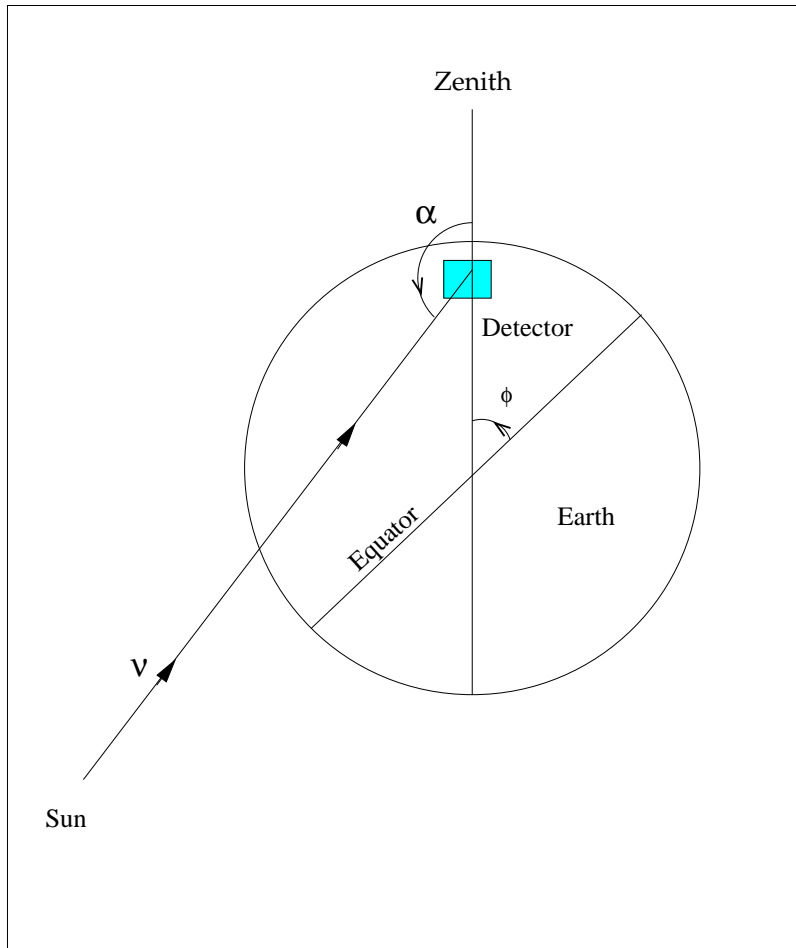


Figure 1

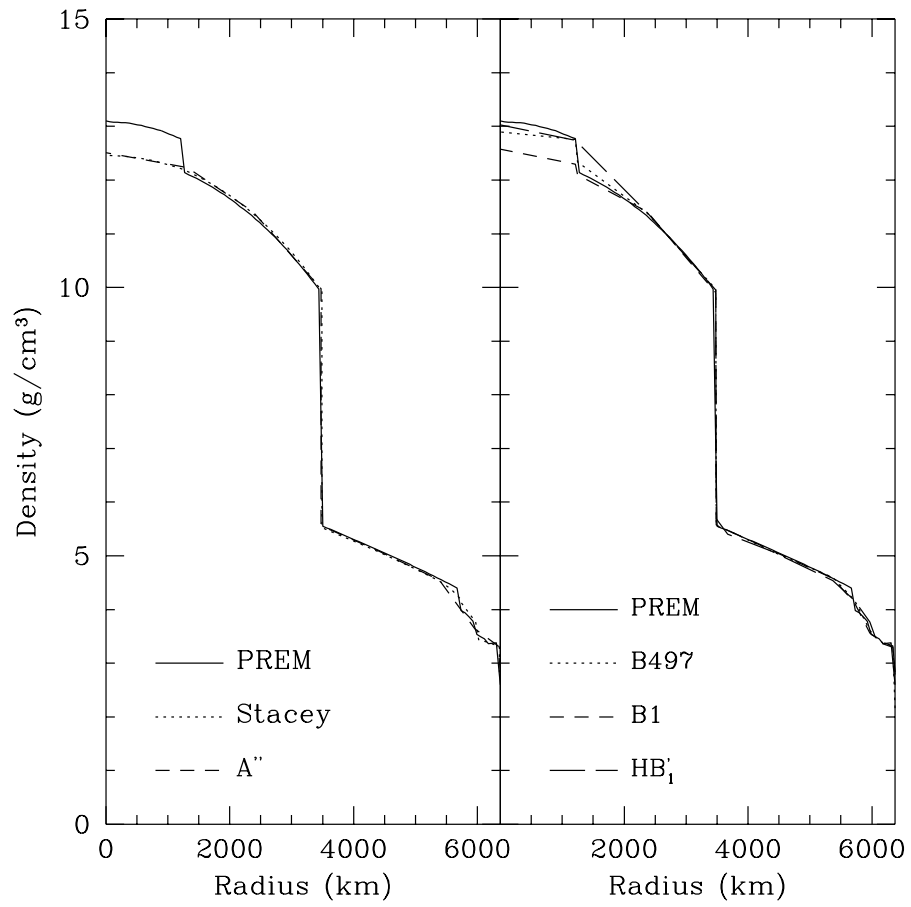


Figure 2

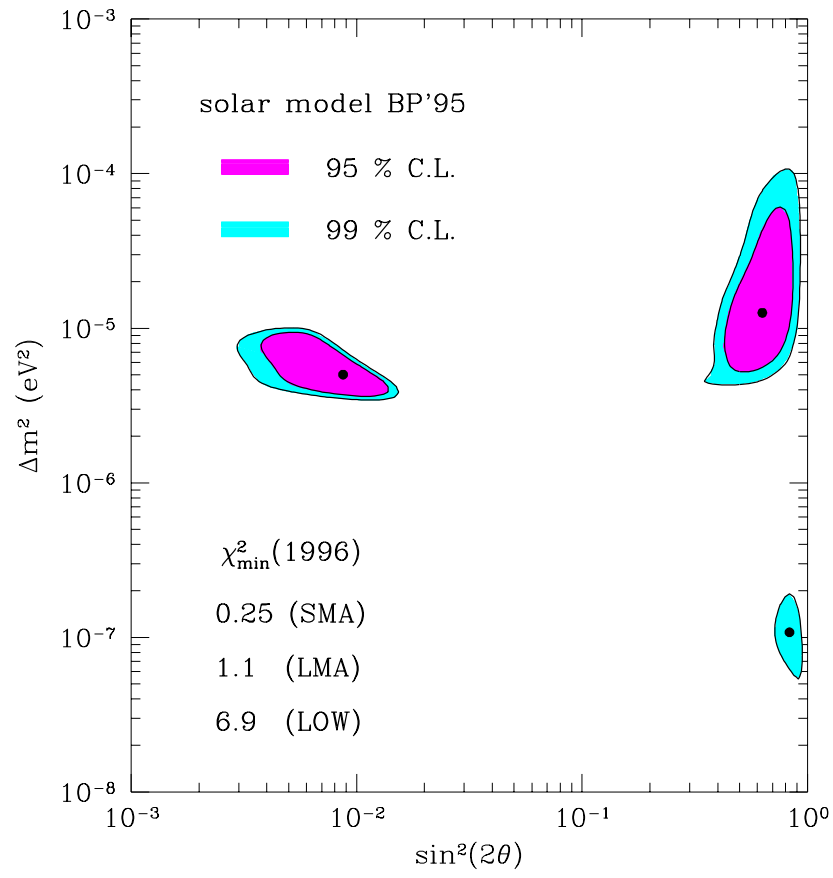


Figure 3

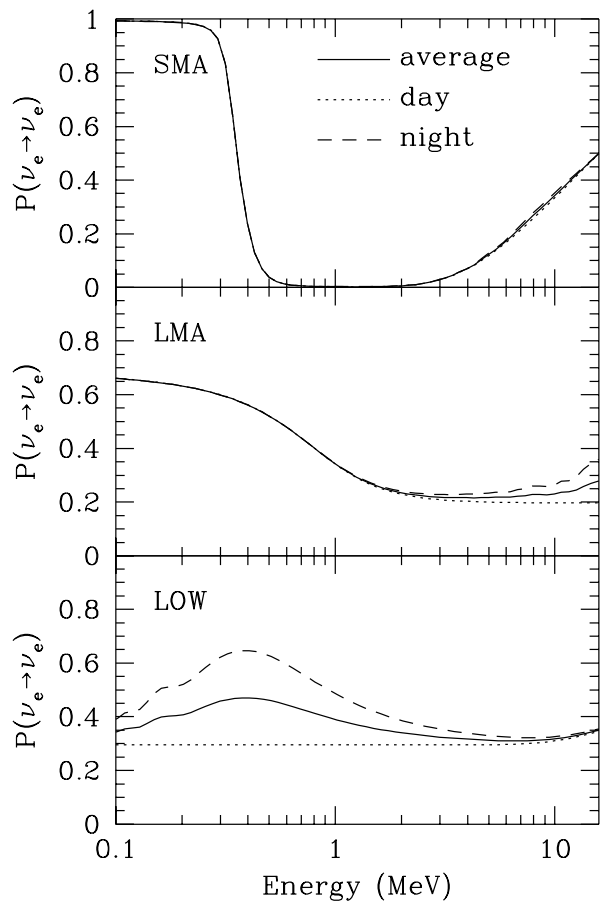


Figure 4

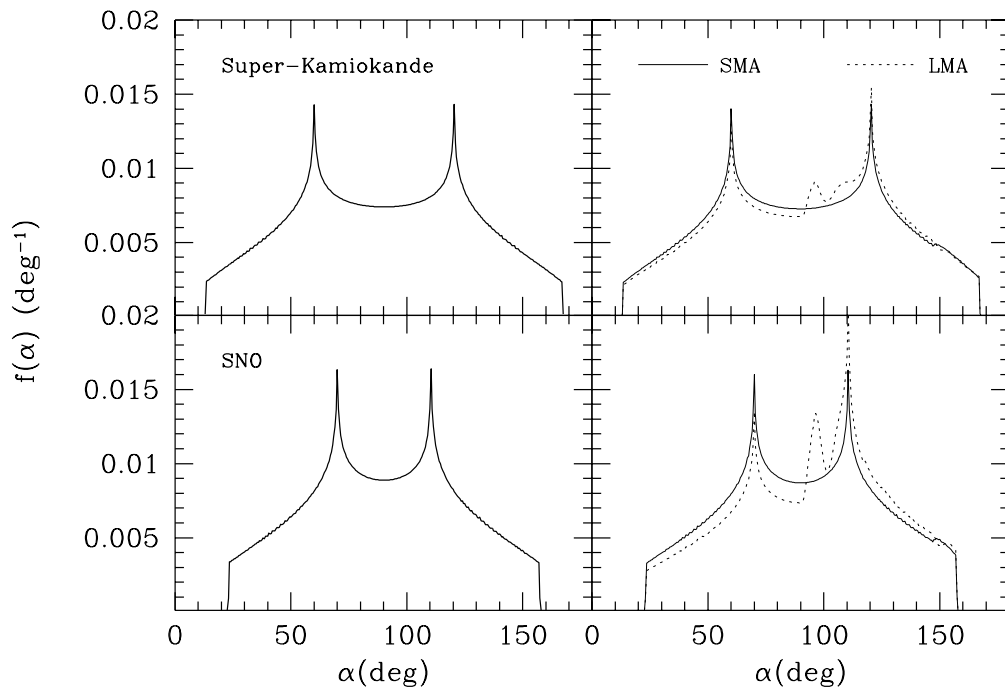


Figure 5

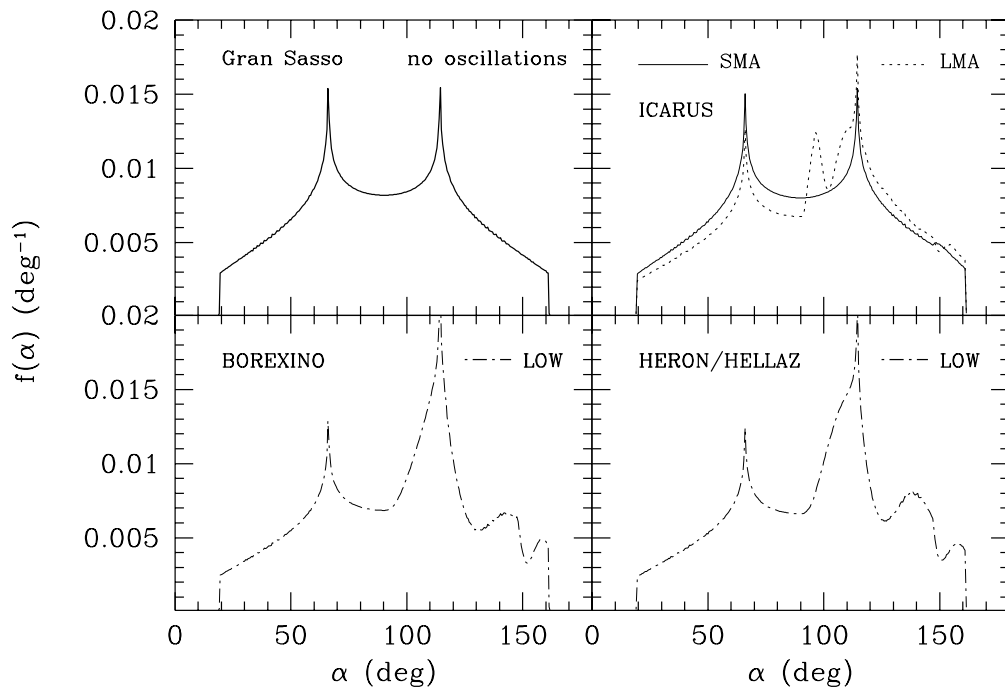


Figure 6

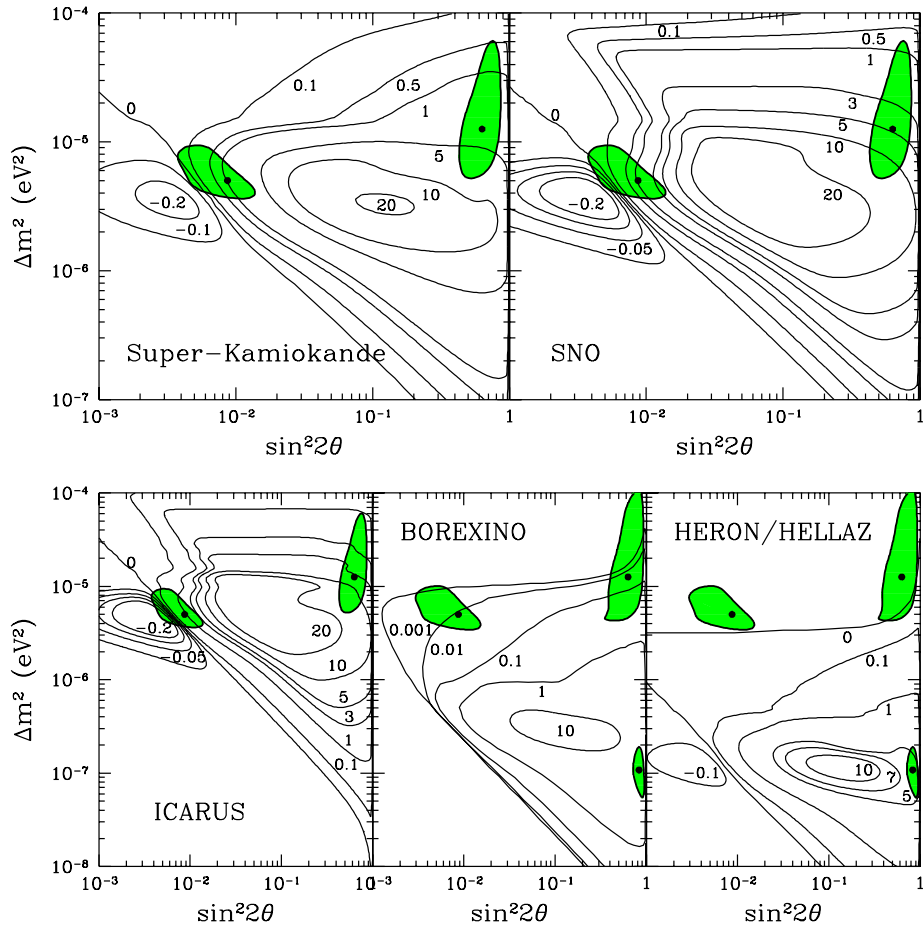


Figure 7

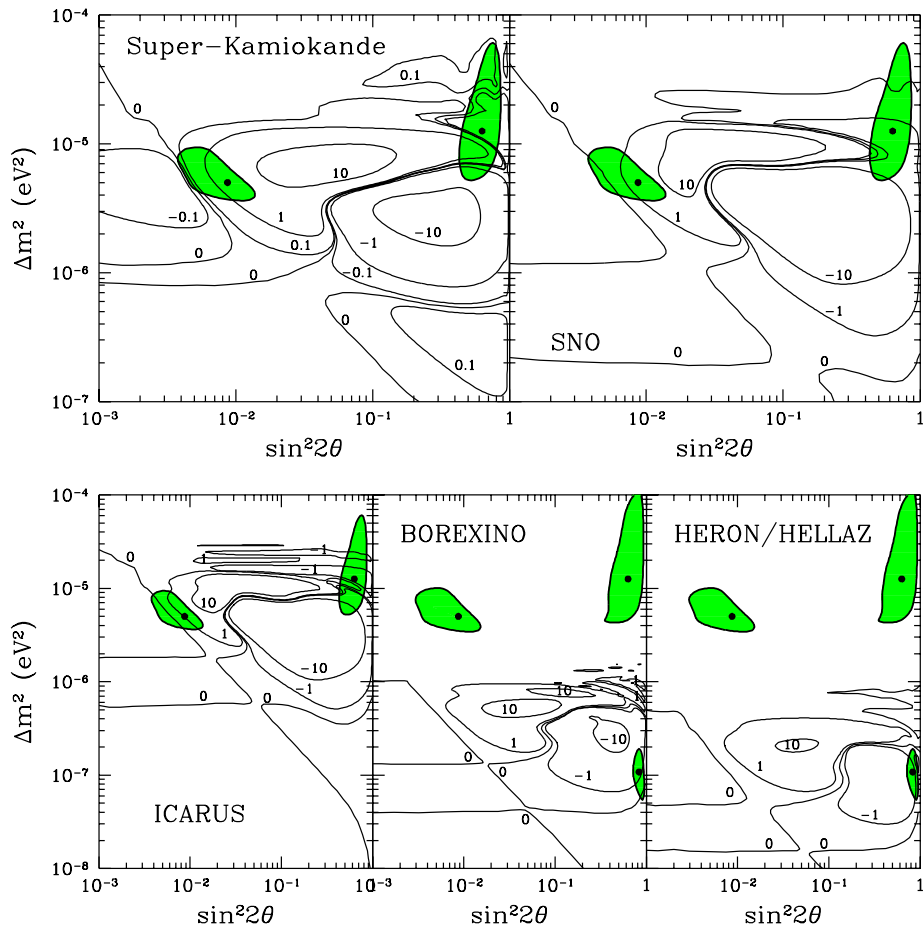


Figure 8

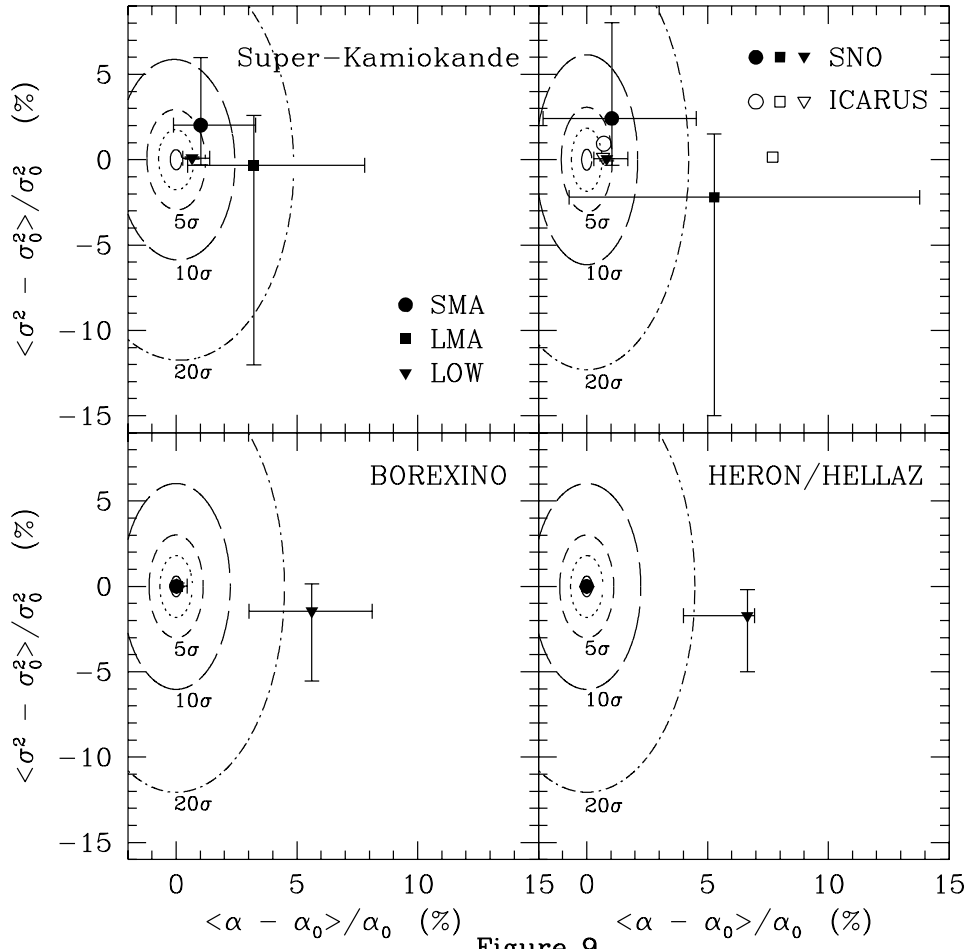


Figure 9

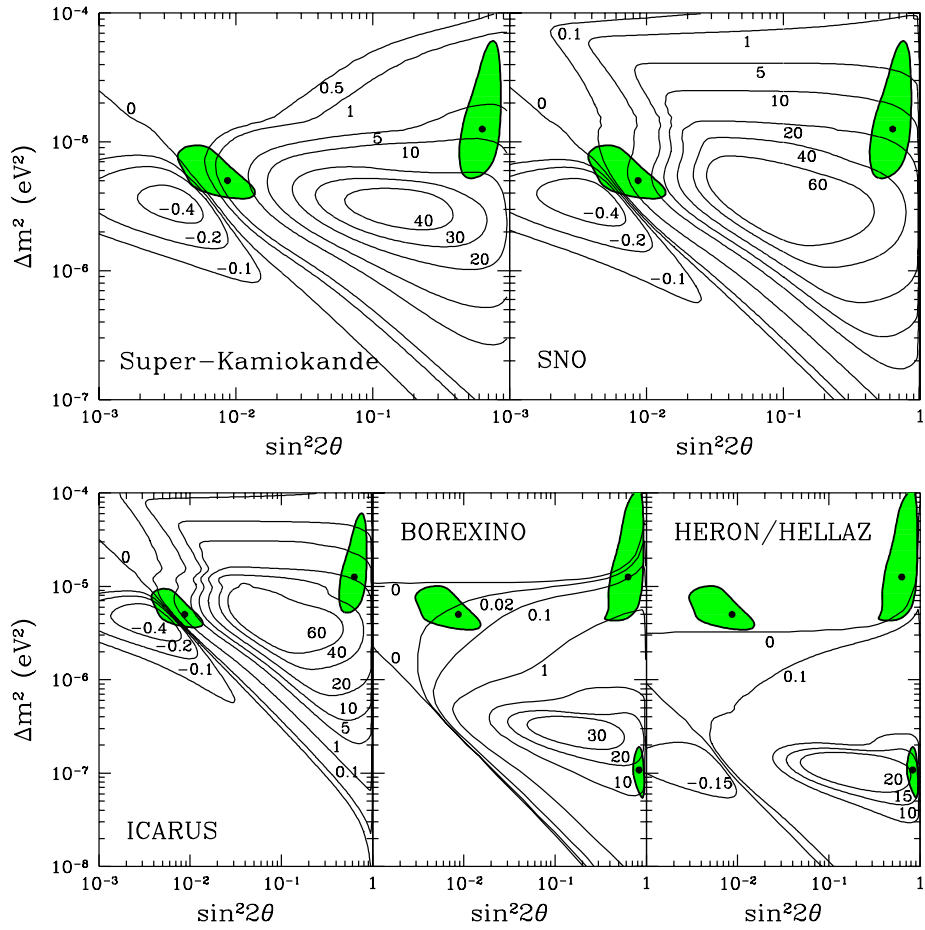


Figure 10

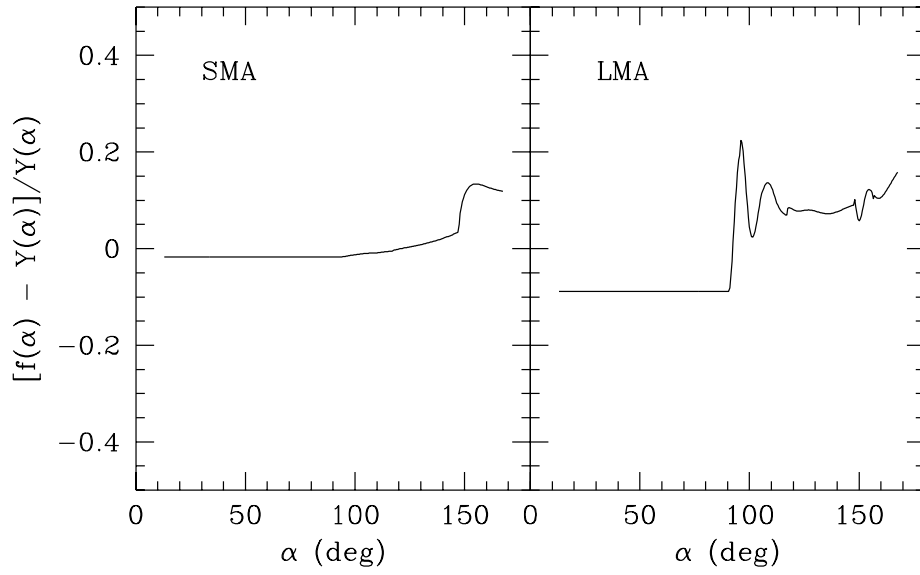


Figure 11

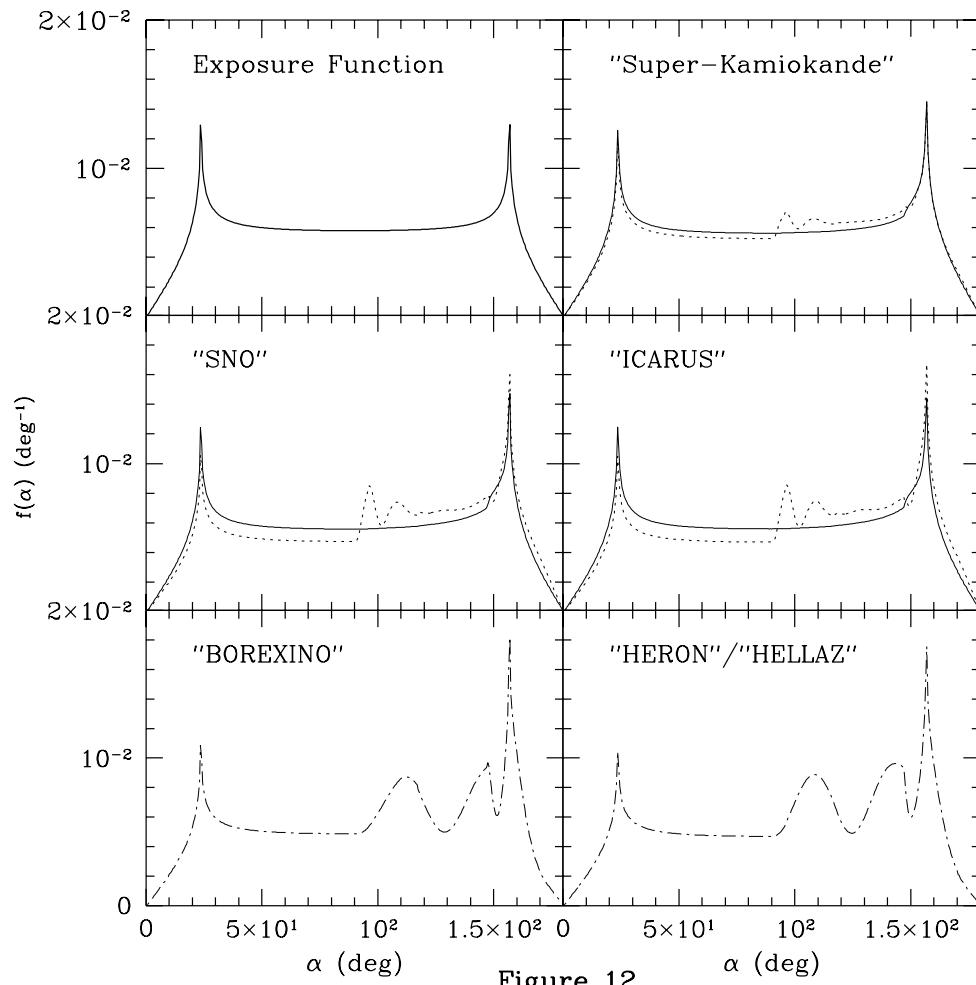


Figure 12

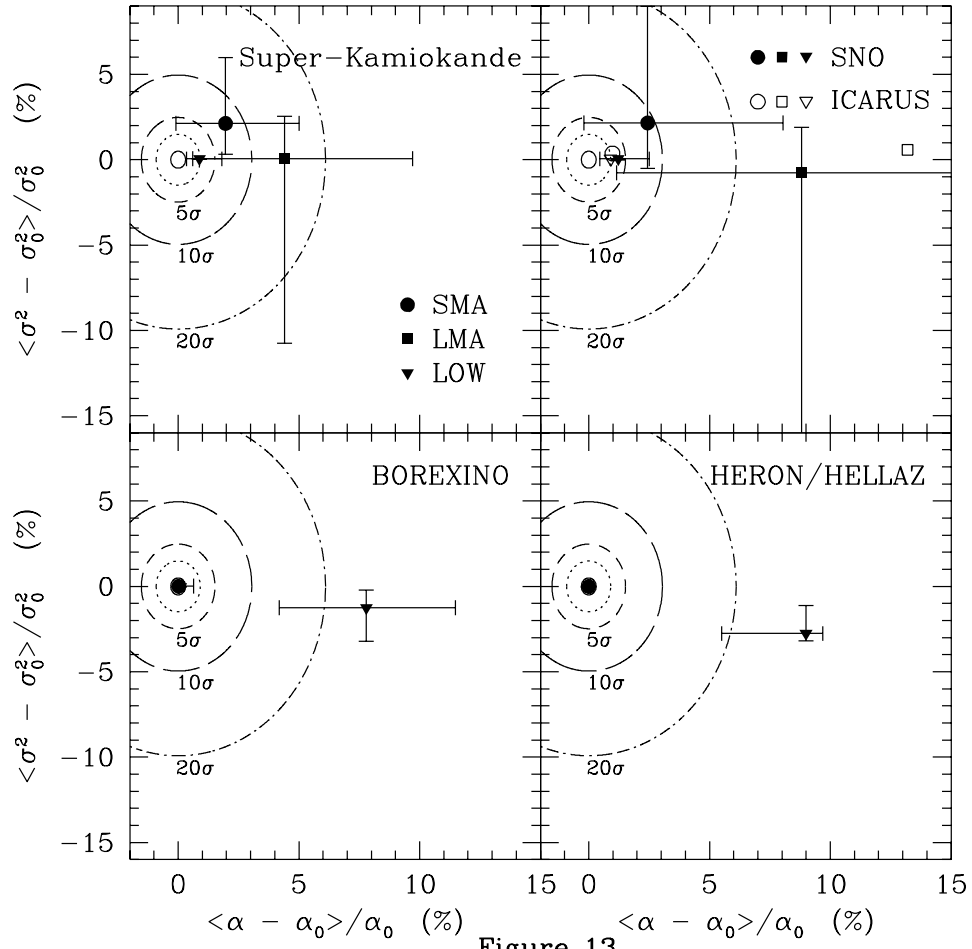


Figure 13